LAWRENCE TECHNOLOGICAL UNIVERSITY

EVALUATION AND ANALYSIS OF DECKED BULB T BEAM BRIDGES

Submitted to

MICHIGAN DEPARTMENT OF TRANSPORTATION
IOWA DEPARTMENT OF TRANSPORTATION
MINNESOTA DEPARTMENT OF TRANSPORTATION
WISCONSON DEPARTMENT OF TRANSPORTATION
OREGON DEPARTMENT OF TRANSPORTATION

Research Administration
Bureau of Field Services
Transportation Pooled Fund Program, Federal Project Number: TPF-5(254)

By

Nabil F. Grace, PhD, P.E., Project Investigator
Mena Bebawy, PhD, Co-Project Investigator

Department of Civil Engineering
Lawrence Technological University
Southfield, MI 48075-1058, U.S.A.

March 2015

TECHNICAL REPORT DOCUMENTATION PAGE

1. Report No. RC-1620	2. Government Accession No.	3. MDOT Project Manager David Juntunen
4. Title and Subtitle Evaluation and Analysis of Decked Bulb T Beam Bridge		5. Report Date March 2015
7. Author(s) Dr. Nabil Grace, Dr. Mena Bebawy, and Marc Kasabasic		6. Performing Organization Code
9. Performing Organization Name and Address Center for Innovative Material Research (CIMR), Dept. of Civil Engineering, Lawrence Technological University, 21,000 West Ten Mile Road, Southfield, MI-48075		8. Performing Org. Report No.
12. Sponsoring Agency Name and Address Michigan Department of Transportation (MDOT) Construction and Technology Division P.O. Box 30049 Lansing, MI-48909		10. Work Unit No. 11. Contract Number: 2010-0293 11(a). Authorization Number:
15. Supplementary Notes		13. Type of Report & Period Covered Final Report, Oct., 2011-Mar. 2015 14. Sponsoring Agency Code

16. Abstract

A new corrosion-free decked bulb T beam bridge system has been developed to overcome some of the problems associated with the construction of side-by-side box beam bridges such as the lack of inspection space between beams and the longitudinal deck cracking. The new bridge system is reinforced and prestressed with carbon fiber reinforced polymer (CFRP) materials instead of the conventional steel reinforcement. In addition, the longitudinal keyways between the top flanges of the beams are grouted using ultra-high performance concrete (UHPC) instead of conventional non-shrink grout. The top flange of the beams with the UHPC shear key joints substitutes the need for a cast-in-place deck slab, a technique that saves time and labor at construction site and ensure the quality control of the product. Through this research project, an experimental investigation and a numerical analysis were conducted to confirm the superiority of the new system. The experimental investigation included the flexural and shear testing of five control beams and a complete bridge model as well, while the numerical analysis was developed, after verification, to evaluate the need for transverse post-tensioning in the system. Results from the experimental investigation and the numerical study indicated that the flexural and shear performance of the new bridge system conforms to the theoretical prediction and the UHPC shear key joints are sufficient to laterally distribute the loads across the bridge width. No signs of longitudinal cracks were observed over the shear key joints of the bridge model even when loading an exterior beam to twice its load carrying capacity. In addition, the CFRP reinforcement was proven to be a proper alternative to steel reinforcement in decked bulb T beams. No premature failure or un-predicable behavior was experienced. The study also showed that a transverse post-tensioning may not be necessary for the system provided that the shear key joints are properly constructed using UHPC. Overall, it can be concluded that decked bulb T beam bridge system with CFRP reinforcement and UHPC shear key joints is an excellent alternative for side-by-side box beam bridge system that promotes expedited construction, access to inspection, reduced maintenance work, and an effective approach to eliminate the longitudinal deck cracking problem.

17. Key Words Decked bulb T beam, bridges, transverse post-tensioning, longitudinal cracks, transverse diaphragms, ultra high performance concrete. CFRP prestressing strands, Un-bonded strands	18. Distribution Statement No Restrictions. This document is available to the public through the Michigan Department of Transportation (MDOT).		
19. Security Classification (Report) Unclassified	20. Security Classification (Page) Unclassified	21. No. of Pages	19. Price

EXECUTIVE SUMMARY

The side-by-side box beam bridge system has been used extensively since 1950s as one of the preferred precast prestressed bridge systems. This is because of its shallow depth, aesthetic appearance, fast and easy construction, needless deck formwork on site, and significant torsional capacity. However, in the last few decades, problems started to emerge with the use of this bridge system, most notably the development of longitudinal deck cracks between the box beams. These cracks often lead to accelerated deterioration of the superstructure as water and deicing chemicals seeps through them into the sides of the beams. With the lack of space between box beams hindering the full inspection and maintenance, early treatment of the deterioration becomes unfeasible. Subsequently, the structural integrity of the bridge becomes comprised over time.

While, extensive effort has been deployed to mitigate the longitudinal deck cracking problem in side-by-side box beam bridges by providing adequate transverse post-tensioning system, the lack of space for inspection and maintenance between beams remains unaddressed. Therefore, this research investigation aims at addressing this problem by offering an alternative to the side-by-side box beam bridge system. The proposed system consists of precast prestressed decked bulb T beams reinforced and prestressed with carbon fiber reinforced polymer (CFRP) materials instead of the conventional steel reinforcement. The new system does not have a separate deck slab. Instead, the flanges of the bulb T beams are connected together to form a smooth riding surface. To ensure a proper lateral load distribution between the beams and to minimize the potential of longitudinal deck cracking, the connection between the beams is cast using ultra-high performance concrete (UHPC) instead of the conventional non-shrink grout that is typically used for cold connections. In addition, the beams are also connected together using transverse diaphragms. Part of the diaphragm may be pre-cast as an integral body of the beam and then the diaphragms are connected together using UHPC. Furthermore, the diaphragms are provided with conduits for possible un-bonded transverse post-tensioning if deemed necessary by the designer, or for future needs.

To verify the concept of the new bridge system, an experimental investigation accompanied by a numerical study was conducted. The experimental investigation included the construction and testing of five control decked bulb T beams and a complete bridge model composed of five beams connected together as mentioned earlier. Several loading scenarios were performed on the control

beams and the bridge model. Four control beams were tested to failure under flexural loading setup. One beam was reinforced and prestressed with conventional steel reinforcement while the other three beams were reinforced with carbon fiber composite cable (CFCC) strands with different reinforcement ratios (under-reinforced, balanced, and over reinforced). The four flexurally tested beams were provided with steel stirrups. On the other hand, the fifth beam was provided with CFCC stirrups and tested under shear loading setup to failure. The bridge model was loaded through three states: service, post-cracking, and strength limit states. The loading was performed with and without transverse post-tensioning system. The strength limit state loading of the bridge model was executed by loading the intermediate beam of the bridge model under four-point loading to failure. The loading was performed without transverse post-tensioning leaving only the UHPC shear keys to distribute the loads to the adjacent beams.

The numerical investigation included two stages of analysis: verification and parametric study. Through the verification stage, the results from the experimental investigation were used to verify the accuracy of the analysis and to adjust different input parameters of the developed numerical model. After adequate confidence was established in the analysis, the second stage was initiated and included modeling prototype decked bulb T beam bridges with widths ranging from 24 ft to 78 ft and spans ranging from 50 ft to 100 ft. The main target of the study was to establish the proper number of transverse diaphragms and to establish the level of transverse post-tensioning force to ensure the integrity of the superstructure and the mitigation of the longitudinal deck cracking. In addition, bridge models with skew angle were also generated to evaluate the relationship between the skew angle and the transverse post-tensioning system.

The experimental investigation and the numerical analysis revealed that decked bulb T beam bridge system is an excellent alternative to side-by-side box beams. It offers the necessary inspection space between beams and maintains its structural integrity to failure. The study also revealed that transverse post-tensioning may not be necessary if the bridge system is provided with adequate number of diaphragms and the connection between the beams are properly constructed using UHPC. Finally, CFCC materials demonstrated its potential as a replacement of steel strands, where corrosion of reinforcement is an issue. The failure loads in all test beams and bridge model surpassed those anticipated by calculations and no premature failure or any unpredictable behavior was experienced.

TABLE OF CONTENT

LIST OF FIGURES

LIST OF TABLES

CHAPTER 1: LITERATURE REVIEW

1.1 Overview

According to Bhide (2008), there are more than 150,000 bridges in United States that are structurally deficient or obsolete and more than 3000 new bridges are added each year. Therefore, there is always a call to build better bridges, reduce travel times, and improve rehabilitation techniques. In addition, the bridge rehabilitation process is often faced with strict and tight schedule to avoid possible traffic interruption.

Accelerated bridge construction (ABC) is gaining popularity daily because of its exceptional benefits such as: reducing onsite construction time, minimizing traffic disruption, reducing environmental impact, improving worker and motorist safety, improving constructability, and increasing the quality of the final product. The increased quality of the final product comes as a result of the increased quality control, adequate cure time, ease of access, and controlled environment. Some projects have been executed in different states using some of the ABC techniques. For instance, for the George Washington Memorial Parkway Bridge, in Virginia, the deck was replaced using precast panels in 2002 while the bridge was open for traffic on weekdays. For the Live Oak Creek Bridge, in Texas, 86 full-depth and full-width precast deck panels were erected over the beams using shear studs to form the deck for a 700-ft long, 32-ft wide bridge with a total surface area of around 22,400 ft^2. Fiber reinforced polymer (FRP) deck replacement was employed in the rehabilitation of the Rt. 24 Bridge over Deer Creek, MD in 2001.

Side-by-side precast prestressed box beam bridges are considered one of the most common ABC techniques. They are commonly used in the construction of short and medium-span highway bridges in the United States. The superstructure of a side-by-side box beam bridge can be assembled in a few days and does not require formwork to support the deck slab. However, longitudinal deck cracking between adjacent box beams has been reported frequently in this type of bridge superstructure. For instance, out of 219 adjacent box beam bridges constructed in the state of New York (NYSDOT 1992) between 1985 and 1990, 101 bridges exhibited longitudinal deck cracking that extended as far as from support to support. Deck cracking was identified as one of the major causes for deck deterioration in some nation-wide surveys (Grace et al. 2007 and Koch et al. 2001). When deck cracking occurs, water and deicing agents penetrate into the sides

of the box beams and cause spalling of concrete and corrosion of steel reinforcement. Meanwhile, the lack of space between the adjacent beams hinders the regular inspection and maintenance. Consequently, with such accelerated deterioration and absence of preventive maintenance, the bridge engineer is compelled to replace the bridge superstructure after a shorter lifespan.

An appropriate solution for the problem of deck cracking and deterioration in side-by-side box beam bridges can be executed on three different levels: (1) modifying the cross section of the bridge superstructure to allow enough space between the beams for inspection and maintenance, (2) modifying the connection between adjacent beams to ensure the integrity of the superstructure and eliminate the development of longitudinal deck cracking, and (3) replacing the steel reinforcement of the beams with corrosion-free reinforcement such as CFRP reinforcement to extend the service lifespan of the bridge superstructure.

By addressing all three levels of the solution, the current investigation provides the bridge construction community with an innovative corrosion-free ABC system. The outlines for the investigation were established by conducting a detailed literature review presented through the following subsections. The detailed literature review highlights the current challenges associated with the use of side-by-side box beam bridges along with the possible solutions.

1.2 Side-by-side box beam bridges

Precast prestressed concrete side-by-side box beams are widely used in short and medium-span highway bridges because of their simple design, low life cycle costs, quick and easy construction, and low depth-to-span ratio. Side-by-side box beam bridges are strong, tough, durable, and attractive in appearance. Different techniques can be used in side-by-side beam bridge construction. For instance, in Michigan, the superstructure (Figure 1.2-1) is constructed by: (1) placing precast, prestressed concrete box beams adjacent to each other with gaps of a width ranging from 1.5 in. to 3.0 in. (38 mm to 76 mm), (2) filling the gaps between the box beams with a non-shrink grout to form interlocking full-depth shear keys, (3) applying transverse post-tensioning (TPT) through transverse diaphragms, and (4) casting a 3 to 6-in.-thick reinforced concrete deck slab. Successful integration of the box beams, shear keys, transverse post-tensioning, and the deck slab enables the bridge to behave monolithically.

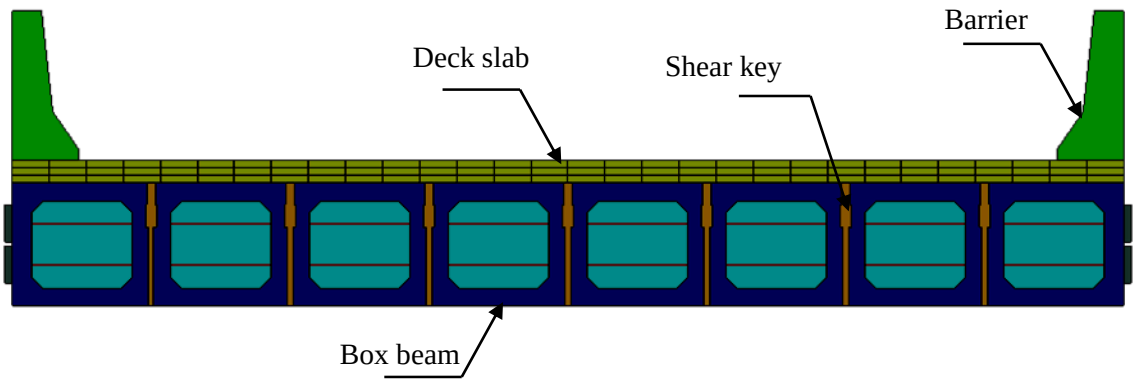

Figure 1.2-1 Typical cross section of side-by-side box beam bridges

The development of longitudinal cracks in the deck slab between the box beams is a major concern (Figure 1.2-2 and Figure 1.2-3) and is frequently reported by inspectors (MDOT 2005 and Lall et al. 1998). For instance, in 1990, an investigator from New York State Department of Transportation reported longitudinal cracks over the concrete overlay shortly after construction. A survey was conducted immediately after the report and included 219 bridges constructed between the years 1985 and 1990 in the state of New York. The results from the survey indicated that 54 % of the bridges built within the given period experienced longitudinal cracking as shown in Table 1.2-1 (Lall et al. 1998). The survey also indicated that longitudinal cracks extended from support to support in many bridges with a crack width in a range of 1/32 to 1/16 in.

Figure 1.2-2 Crack development along the joints in side-by-side box beam bridges

Table 1.2-1 NYSDOT survey for box-beam bridges in 1990 (Lall et al. 1998)

Year built	No. of bridges inspected	No. of bridges with longitudinal cracks	Percent Cracking
1985	36	22	61
1986	34	18	53
1987	36	21	58
1988	33	15	45
1989	34	19	56
1990	14	6	43
Total	187	101	54

Figure 1.2-3 Deterioration of box beams at the shear key joints

Based on the above survey and investigation, NYSDOT concluded that the longitudinal cracks developed due to differential rotation of the beams and the shear key joints were incapable of restraining the differential rotation. In addition, it was concluded that the location of transverse post-tensioning tendons and the number of tendons were also important factors to avoid longitudinal cracking. Furthermore, the research report by NYSDOT suggested that improper location of post-tensioning tendons may lead to the application of eccentric forces on box-beams, which causes differential rotation of the bridge model and results in longitudinal cracking.

Gilbertson et al. (2006) attributed the development of longitudinal cracks to the improper and irregular maintenance along with improper construction techniques. On the other hand, Martin and Osborn (1983) attributed the development of cracks to the poor design of the joints, which degrades their ability to transfer both bending and shear and avoid differential rotation between the bridge components. This was restated by Lall et al. (1998), who assumed that the inability of the longitudinal joints to transfer moments in transverse direction led them to behave as elastic hinges.

Hlavacs et al. (1996) conducted non-destructive tests on shear keys by exposing them to environmental and structural cyclic loading and concluded that longitudinal cracks might initiate as early as immediately after casting the shear keys due to thermal strains. These cracks may propagate partially or fully through the shear key joints. In addition, it was seen that the cracks initiated by thermal strain propagated in the longitudinal direction and through the shear key depth after repeated cyclic loading.

Cracking and failure of the shear key joints leads to the failure of the bridge waterproofing system, which in turn allows water and deicing chemicals to penetrate into the sides of the box beams and cause corrosion of the steel reinforcement with associated concrete spalling. Over time, this deterioration requires costly repairs ranging from concrete patching to deck or beam replacement, or in some severe cases to superstructure replacement.

To mitigate longitudinal deck cracking, different methods have been developed to analyze and design the connection between the box beams. For example, Bakht et al. (1983) assumed that the load is transferred from one beam to another primarily through transverse shear, while transverse flexural rigidity may be neglected. El-Remaily et al. (1996) determined the required transverse post-tensioning force based on flexural rigidity and the lateral moment due to moving traffic. The methods used for analyzing the shear key joint assume that traffic loads are responsible for the

initiation and propagation of longitudinal cracks in side-by-side box beam bridges. However, some experimental investigations indicated that stresses associated with thermal gradients were the main cause of crack initiation, while crack propagation was controlled by traffic loads (Miller et al. 1999). A recent experimental/numerical study (Grace et al. 2008) confirmed that temperature gradients initiate the longitudinal shear key cracks, which propagate with applying traffic loads. Grace et al. (2008) recommended adjusting the transverse post-tensioning system based on the bridge geometry in order to mitigate the longitudinal deck cracking between the box beams.

In summary, side-by-side box beam bridges, though very popular and efficient, come along with several durability issues primarily due to the improper design of the connections between the beams and the lack of adequate space between them. This lack of space impedes the procedure of regular inspection and maintenance. In addition, using non-shrink grout for filling the shear keys was proven inadequate through several research and field investigations. Furthermore, in case of beam replacement, the grouted transverse post-tensioning strands are often abandoned. Therefore, even partial maintenance or replacement of side-by-side box beam bridges can be a complex procedure and may jeopardize the structural integrity of the entire superstructure.

1.3 Decked bulb T beam bridges

A bulb T beam bridge superstructure may be regarded as a potential alternative to a box beam bridge superstructure. This type of superstructure has emerged rapidly in bridge design and construction during the last few decades. Several design agencies have implemented bulb T beams in their design guidelines with some differences in dimensions and construction techniques. For example, Utah Department of Transportation (UDOT) uses three classes to categorize bulb T beam bridges according to construction technique. These classes are: (1) Bulb T beams with concrete deck, (2) decked bulb T beams without concrete deck, and (3) post-tensioned bulb T beams with concrete deck and post-tensioning strands. Likewise, Washington State Department of Transportation (WSDOT) provides details for both bulb T beams with deck and decked bulb T beams without decks (WSDOT 2008).

Examples for the construction of decked bulb T beams can be traced back to 1986 with the construction of a six-span prestressed concrete decked bulb T beam bridge in Minnesota (Hill et al. 1988). Each span was assembled with five adjacent decked bulb T beams that had a depth of 40 in. and top flange width of 6 ft. The end spans had a length of 70 ft, while the interior spans had

a length of 85 ft. Steel bars with a diameter of 1.0 in. were used to transversely post-tension the top flange.

In 1987, a 142-ft long three-span continuous decked bulb T beam bridge was built in the Southeast of Forks, Washington over South Fork Hoh River (Owen 1987). The bridge replaced a 22-year old deteriorated wooden bridge. The new bridge deck was composed of three decked bulb T beams with a depth of 42.5 in. (Figure 1.3-1). The beams were designed as simply supported for dead loads and continuous for live loads. The continuity of the spans was achieved by applying post-tensioning force of 300 kips through draped post-tensioned strands (Figure 1.3-2). An intermediate diaphragm made of galvanized steel pipes was placed at the location of the maximum bending moment in each span. In addition, no end blocks were provided at the location of the interior supports.

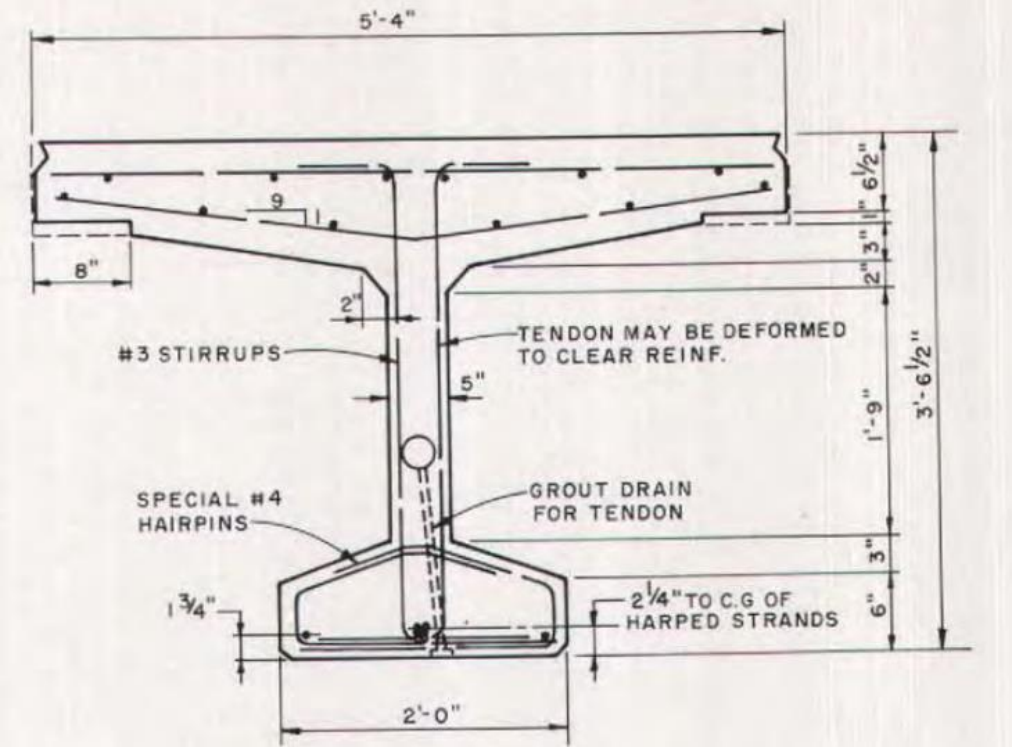

Figure 1.3-1 Cross section of decked bulb T beam used for bridge construction (Owen 1987)

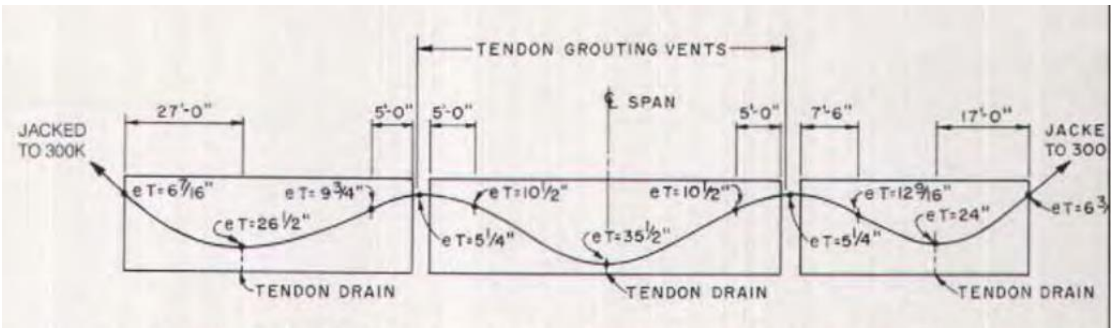

Figure 1.3-2 Layout of postensioning strands in the bridge deck (Owen 1987)

In 2009, a decked bulb T beam bridge was constructed in Kittitas County, WA to replace a deteriorated bridge. The beams were interconnected using welded steel joints. In addition, to overcome longitudinal joint leakage, the new bridge was provided with a waterproof membrane in addition to an asphalt emulsion used to hold the membrane in place.

In spite of their benefits, the use of decked precast, prestressed concrete girders has been limited because of concerns regarding certain design and construction issues that may affect the structural integrity of the bridge system. These concerns include the connections between adjacent units, longitudinal joints, longitudinal camber, cross slope, live load distribution, live load continuity, lateral load resistance, skew effects, maintenance, replaceability and other factors that influence constructability and performance (Oesterle et al. 2009). Therefore, some states (e.g. Washington) impose restrictions on the use of this system for roads with high average daily traffic (ADT) and for continuous bridges.

A recent research project was conducted jointly between the University of Minnesota–Twin Cities and the University of Tennessee–Knoxville. This research project was used to evaluate the performance of cast-in-place connections between decked bulb T beams. The research project investigated different reinforcement details for the connection and different grout materials (French et al. 2011). An experimental phase was executed to test connection specimens under static and cyclic loading. Based on the results of the research project, the research team recommended specific reinforcement configurations and grout materials. However, the realistic performance of the shear key connection was not evaluated. It should be noted that the experimental investigation showed the development of undesirable wide cracks under service loads when high grade steel

reinforcement was used for the connections because a less amount of reinforcement crossed the interface.

Oesterle and Elremaily (2009) focused on the development of design guidelines for precast prestressed decked girder bridges. The guidelines included the design of the longitudinal joints between the flanges of adjacent girders. This was defined as a major issue inhibiting the general use of decked girders. From that research project, an improved joint was proposed. The improved joint included headed reinforcing bars lap spliced to develop moment and shear continuity in narrow grouted joints. The findings of the study indicated that the improved joint detail was viable in transferring the force between adjacent decked bulb T girders.

Through a finite element analysis, Li et al. (2010) studied the effects of adding intermediate diaphragms to the decked bulb T beam bridge system. The research project addressed aspects such as deflections and flexural strains in the beams at the mid-span. Steel and concrete diaphragms were considered. The study showed that at least one intermediate diaphragm should be provided at the mid-span regardless of the diaphragm details, which did not seem to influence the deflection of the girders or the strain level. On the other hand, the influence of having intermediate diaphragms on the deflection of the beams was more prominent in short-span bridge models than in long-span bridge models.

In summary, decked bulb T beam bridges can be a promising technique for ABC if the issues regarding the connection between the beams are fully investigated and resolved. Therefore, special attention is given in the current investigation to the connection design. An in-depth literature review and analysis was performed to evaluate the performance of shear key connections between adjacent decked bulb T beams.

1.4 Shear key joints in decked bulb T beam bridges

The current practice for constructing the shear key joints is to fill the gaps between adjacent precast concrete elements with a no-shrink grout. However, the adequacy of this practice has been critically questioned with the development of longitudinal shear key cracks under high traffic volumes or under harsh environmental conditions (Miller et al. 1999). Some jurisdictions and districts recommend extending the reinforcement from the precast units to form the reinforcement of the shear key connections. However, there was always a concern regarding the development

length of the extended reinforcement because the shear key connection is usually narrow, within the range from 3 to 6 in. wide. Therefore, the extended reinforcement may need to have different configurations to ensure an adequate development length over a relatively narrow connection (Figure 1.4-1 and Figure 1.4-2). Other districts recommend providing welded steel joints at intervals along the span of the bridge (Figure 1.4-3). This practice has often been criticized due to problems associated with the crack development over the distances between the welded steel plates (French et al. 2011).

Figure 1.4-1 Reinforcement configuration for shear key connections (French et al. 2011)

Figure 1.4-2 Headed reinforcement for shear key connections (Oesterle and Elremaily 2009)

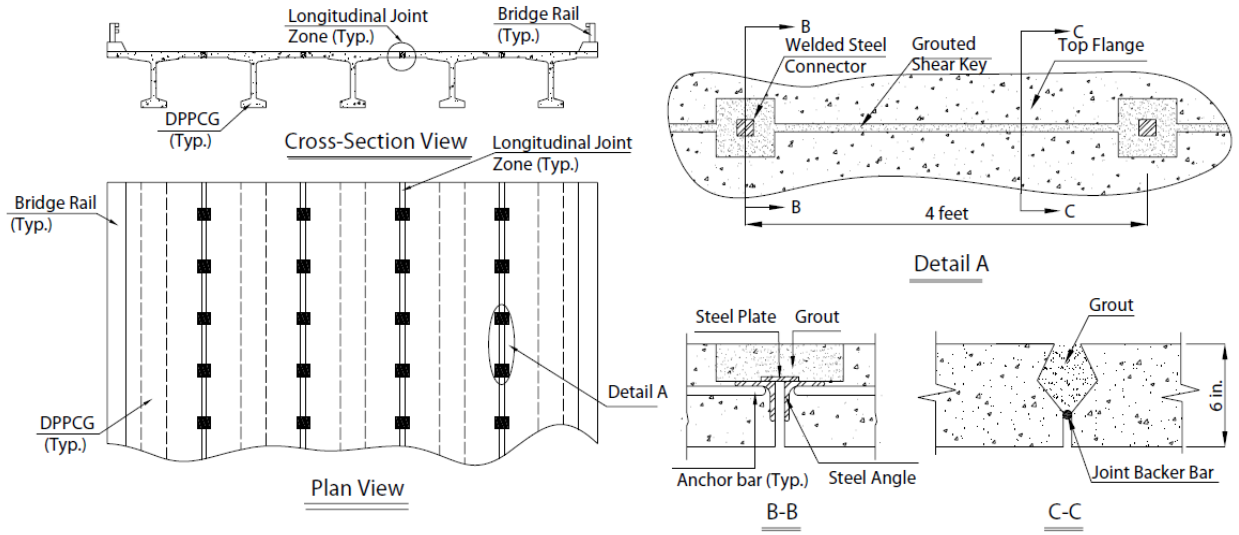

Figure 1.4-3 Former techniques in constructing the connection between decked bulb T beams using welded steel connectors (French et al. 2011)

With the development of advanced engineering materials, alternatives to the non-shrink grout have emerged. A plausible alternative to the non-shrink grout is the ultra-high performance concrete (UHPC). The innovation of UHPC can be traced back to Bache (1981), who developed the approach of manufacturing a tightly packed dense concrete matrix to increase both tensile and compressive strength. Steel fibers are added to overcome the brittleness of the material that arises due to the dense matrix. The dense matrix ensures strong bond to the fibers that increases the post cracking strength as long as high strength fibers are used. UHPC is designed for use in the elastic stage so the fibers action becomes effective only when the ultimate limit state is approached. UHPC is slightly heavier than normal weight concrete with an average unit weight of 156 lb/ft^3.

The uniaxial stress-strain behavior of UHPC differs from conventional concrete in several ways. Most notably, the UHPC can achieve a compressive strength of 26 ksi (Figure 1.4-4) and direct tensile strength in excess of 1.5 ksi. UHPC exhibits tensile capacity exceeding the initial tensile cracking and maintains this tensile capacity until pullout of the fiber reinforcement. At fiber pull out, the average tensile strain of the UHPC is 0.007 (Graybeal 2006). In addition, when subjected to compression, UHPC exhibits a significantly more linear stress-strain response than that observed in normal weight concrete.

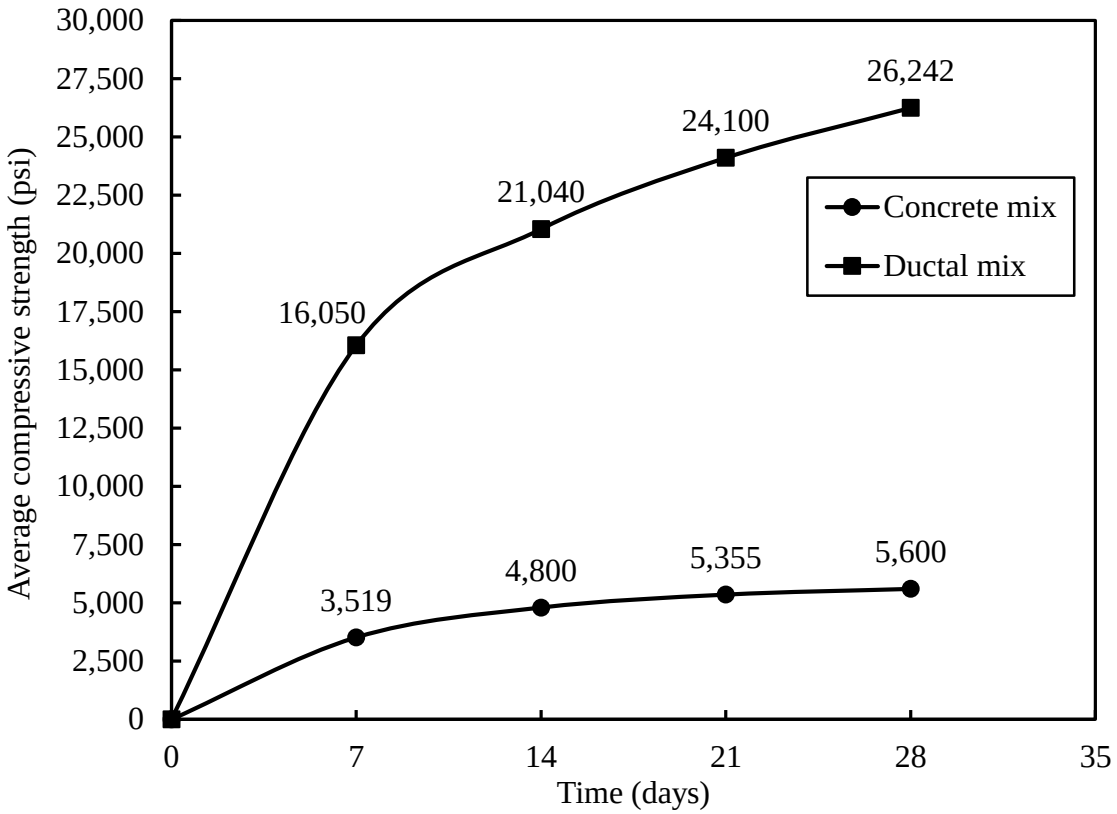

Figure 1.4-4 Compressive strength of UHPC vs. compressive strength of regular-mix concrete

A typical composition of UHPC is shown in Figure 1.4-5. This innovative material can be classified as a reactive powder concrete. It is a special type of ultra-high-strength superplasticized fiber-reinforced silica fume concrete, with improved homogeneity. Traditional coarse and fine aggregate are replaced by fine sand with particle sizes in the range of 4-16 thousands of an inch (Shaheen et. al., 2007). A commercially available UHPC is manufactured by Lafarge under a commercial name Ductal®. The components of Ductal® are micro silica, silica fumes, cement, quartz sand, superplasticizer, and short fibers. Steel or polyvinyl alcohol (PVA) fibers have been used successfully with the dense concrete mix. However, durability issues related to the corrosion of steel fibers remain a concern.

Through various experimental investigations, Ductal® has shown exceptional high strength and durability (Perry and Zakariasen 2004). For instance, Ductal® can achieve a compressive strength ranging from 22 to 28 ksi, a flexural strength ranging from 2.2 to 3.6 ksi, and a modulus of elasticity ranging from 6,500 to 7,300 ksi. Ductal® has a relative dynamic modulus (RDM) of 112 % under

freeze/thaw cycles (ASTM C666). It also has abrasion loss of less than 0.026 oz (ASTM C944) and chloride ion (CL^-) permeability less than 0.10 lb/yd^3 (AASHTO T259).

Small brass-coated steel fibers with a diameter of 0.008 in and a length of 0.5 in. are commonly used as fiber reinforcement in Ductal®. Synthetic fibers such as poly-vinyl alcohol have also been used (Parsekian et al. 2008). Besides their structural performance, the added fibers enhance the overall durability of the mix by changing the cracking pattern from a few large cracks to many small cracks. Wide cracks allow for intrusion of aggressive solutions. However, small and tight cracks prevent water and solutions from seeping into the concrete and thereby reduce the permeability of the element. The low permeability of Ductal® enhances various durability aspects such as the resistance to freeze and thaw cycles, which in turn leads to an extended service life and reduced maintenance costs.

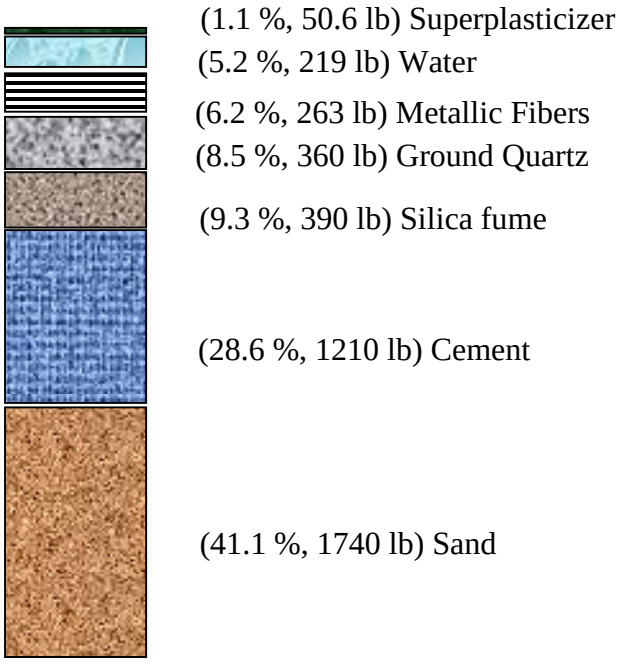

Figure 1.4-5 Components of UHPC Ductal® by weight for one cubic yard

UHPC was first used in the bridge industry in the construction of a pedestrian bridge in Quebec, Canada in 1997. Another pedestrian bridge in South Korea and a highway bridge in France were also constructed using UHPC in 2002. In 2006, the Iowa DOT worked cooperatively with Wapello County and Bridge Engineering Center (BEC) at Iowa State University (ISU) to design, construct, and evaluate the first UHPC bridge built in the United States. The simply supported bridge had a span of 110 ft and a deck width of 27 ft. The bridge was constructed using three UHPC modified I-shaped girders (Figure 1.4-6 and Figure 1.4-7). Other components of the bridge, including the deck slab and diaphragms, were constructed using a conventional concrete mix. The second use of UHPC beams in the U.S.A. was for the Jakway Park Bridge in Buchanan County, Iowa. Three UHPC Π-shaped beams with a length of 51ft were used to construct the center span of this three-span bridge. The bridge was opened for traffic in 2008.

Figure 1.4-6 Iowa UHPC Mars Hill Bridge, Ottumwa, Iowa (Iowa DOT 2011)

Figure 1.4-7 Flexural/shear load testing of a full-scale I girder beam (Iowa DOT 2011)

The use of UHPC in field-cast deck connections has drawn the attention of many research groups. The concept of using UHPC in shear key connections takes advantage of the high strength material in reducing the development length of the reinforcement and thereby, reducing the overall width of the connection. In addition, cracks are significantly controlled and mitigated due to the high strength of the material. Unlike non-shrink grout materials, UHPC can achieve excellent bond strength with the adjacent precast element. Therefore, the development of interface cracking becomes less likely. Besides, because of the low permeability of UHPC, shear key connections made from UHPC are expected to last longer than grouted shear keys.

UHPC was used to form deck connections between precast deck panels such as those in Rainy Lake Bridge (2006) and Chukuni River Bridge (2010) or to form shear key connections between adjacent box beams such as those in Sunshine Greek Bridge (2007), Hawk Lake Bridge (2008), Buller Greek Bridge (2009), Log River Bridge (2009), Eagle River Bridge (2009), and Wabigoon River Bridge (2010). The Ministry of Transportation of Ontario (MTO) is the leader in the deployment of field-cast UHPC connection technology. By the end of 2011, the MTO completed the construction of sixteen bridges with UHPC used in the connections between precast concrete elements.

The Rainy Lake Bridge is a highway bridge over the Canadian National Railway (CNR) at Rainy Lake, near Fort Frances, Ontario. This skewed simply supported bridge was originally built in 1963 with a span of 80 ft and a deck width of 36 ft. The superstructure of the bridge was composed of five steel plate girders supporting a 7 in. thick cast-in-place deck slab. In 2006, a project was conducted to replace the deteriorated cast-in-place bridge deck with new precast deck units. No transverse post-tensioning was allowed due to technical and economic factors. In addition, it was mandatory to keep the bridge open to traffic during the retrofit. The new deck replacement was formed of precast rectangular deck panels with dimensions of 19 ft × 12 ft × 9 in. The panels were reinforced with Glass Fiber Reinforced Polymer (GFRP) bars as top mat reinforcement and conventional steel bars as bottom mat reinforcement. The new deck system was designed to be fully composite with the existing steel girders. This was accomplished using standard Nelson shear studs welded to the top flanges of the girders at the precast panel pockets. The shear studs were fixed to the panels using UHPC. In addition, precast continuity was provided

by the field-cast UHPC construction joints as shown in Figure 1.4-8 and Figure 1.4-9 (Perry et al. 2009).

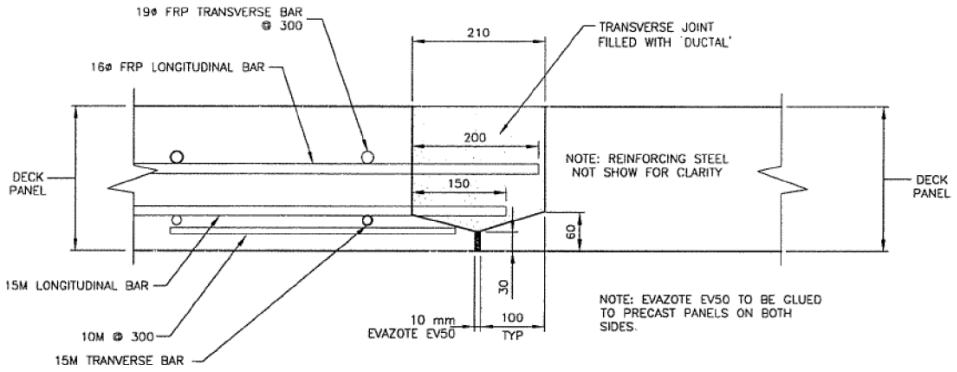

Figure 1.4-8 Details of transverse joints between precast deck panels in Rainy Lake Bridge, ON, Canada (Perry et al. 2009)

Figure 1.4-9 Joints ready for casting (left) and filling the joints with UHPC (right) in Rainy Lake Bridge, ON, Canada (Perry et al. 2009)

The Hawk Lake Bridge (Figure 1.4-10) carries Trans-Canada Highway 17 traffic over the Canadian Pacific Railway. It is a single-span bridge with a span length of 89.3 ft and a deck width of 45.3 ft. The bridge superstructure was composed of 12 adjacent precast box girders connected

together using shear key joints made of Ductal®. Due to the remote location of the bridge, the UHPC Ductal® was mixed on site and thermal blankets and heated water coils were used to ensure proper curing at night-time temperatures (32° to 59° F). The average 28-day concrete compressive strength of the field-cured UHPC joints was 21.0 ksi.

Figure 1.4-10 Hawk Lake Bridge, ON, Canada

The Eagle River Bridge (Figure 1.4-11) carries Highway 17 over Eagle River in Ontario, Canada. The superstructure of this bridge consists of three spans with each span constructed with 12 side-by-side precast prestressed box beams. The box beams were reinforced with V-ROD® #5 and #8 bar and carbon bar for pre-stressing. Also, #6 bars were used in the approach slabs. The continuity for live loads between the three spans was achieved by grouting the joints between the spans using UHPC in addition to grouting the longitudinal joints between the box beams.

Figure 1.4-11 Construction of Eagle River Bridge, Ontario Canada

New York State Department of Transportation (NYSDOT) employed UHPC in two projects. The first project was the Route 31 Bridge in Lyons, New York (Figure 1.4-12 and Figure 1.4-13). In this project, a deteriorated superstructure was replaced with a new superstructure composed of eight 41-in. deep decked bulb T beams. The new superstructure was simply supported over a span of 87.4 ft with a total deck width of 42.8 ft. The beams were interconnected at their top flanges using longitudinal UHPC shear key connections with a width of 6 in. and a depth of 6 in. To provide reinforcement through the connections, straight epoxy-coated reinforcing bars were projected from precast beams into the connection. After adjusting the cambers in the beams and forming the connections, the UHPC was mixed and cast. After casting, the exposed surfaces were covered to prevent dehydration and the UHPC was then allowed to cure under ambient environmental conditions. After curing, the bridge deck surface was ground. Finally, a waterproof membrane and asphalt overlay were installed.

Figure 1.4-12 Longitudinal connections in Route 31 Bridge in Lyons, New York (Graybeal 2010)

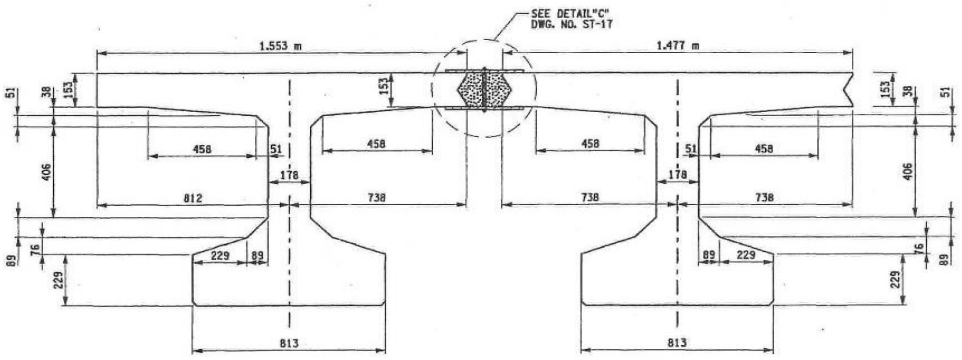

Figure 1.4-13 Dimensions and shear key connection in NYS DOT bridge replacement for Route 31 over Canandaigua outlet (Graybeal 2006, dimensions are in mm)

The second project was the replacement of the Route 23 Bridge over the Otego Creek in Oneonta, New York. The bridge deck construction included the use of precast deck panels and field-cast UHPC connections. After setting the precast panels on the steel girders and forming the connections, the UHPC was mixed, cast and allowed to cure at the ambient environmental conditions (Figure 1.4-14). After curing, a 1.6 in. minimum thickness concrete overlay was provided for a smooth riding surface.

Figure 1.4-14 Field-casting of UHPC, Route 23 Bridge in Oneonta, New York (Graybeal 2010)

The Virginia Department of Transportation (VDOT) has used UHPC with steel fibers in the construction of five beams located in one of ten spans of the bridge on Route 624 over Cat Point Creek. Each span of the bridge had a length of 81.5 ft and was composed of five 45-in. bulb T beams. A test beam with a span of 20 ft was also fabricated and tested to failure (Figure 1.4-15). The beams had longitudinal strands but no shear reinforcement was provided. Test beam results indicated satisfactory load-carrying capacity. Preparation of the beams involved a longer mixing time and a two-stage steam curing to ensure optimum concrete properties. Testing of specimens at the hardened state showed that UHPC has high strength and high durability attributed to a very low water–cementitious materials ratio, low permeability, high resistance to cycles of freezing and thawing, and tight cracks (Ozyildirim 2011).

Figure 1.4-15 Building and testing UHPC bulb T beam (Ozyildirim 2011)

An experimental study was performed at Michigan Technological University (MTU) to evaluate the bond strength between an UHPC overlay and normal concrete substrate with different types of surface textures including smooth, low roughness, and high roughness texture. Slant shear (ASTM C 882-05) and splitting prism (modified ASTM C 496) tests were performed to quantify the bond strength under combined compression/shear and indirect tension. Test results demonstrated that under compressive loading (slant shear test), the bond strength is greater than the strength of the substrate, provided that a surface texture greater than the standard smooth finished mortar surface is used. Splitting prism test results were not highly sensitive to the surface roughness. In both cases, the measured bond strengths fell within the ranges specified in the ACI design guidelines for the Selection of Materials for the Repair of Concrete. The study concluded that UHPC provides adequate bond performance for a variety of substrate surface conditions.

Graybeal (2010) performed a study to evaluate the performance of UHPC deck connections under cyclic and static loading. Four 7.8-in. thick specimens were constructed to simulate transverse deck connections with different reinforcement layouts. Two 6-in. thick specimens were constructed to simulate longitudinal deck connections. The specimens had a rectangular shape with dimensions of 94.5 in. × 84.7 in. The UHPC connection was placed at the mid-span of each specimen with a width of 6 in. All the specimens were loaded at their mid-spans with a point load near the connection (Figure 1.4-16). The cyclic loading test included applying a minimum of two million cycles of loading/unloading at a load level just below the cracking strength of the specimen and a minimum of five million cycles of loading/unloading at a load level above the cracking

strength of the specimens. After completion of the load cycles, the specimens were loaded with a static load to failure. Overall, it was determined that the performance of UHPC field-cast connections in this experimental investigation surpassed that anticipated in monolithic decks with no connection debonding. However, it was noted that the connection was neither susceptible nor immune to water leakage. In case of loading beyond the cracking strength, it is expected that flexural cracks will develop near the connection and water leakage became inevitable. This is an issue in both cast-in-place deck slabs and precast deck slabs with connections.

Figure 1.4-16 Testing of UHPC shear key joints between deck panels (Graybeal 2006)

The possible need for transverse post-tensioning (TPT) to secure the UHPC shear key connections in decked bulb T beams has not been investigated. Based on earlier studies performed on side-by-side box beam bridge (Grace et al. 2008), it was determined that TPT arrangement prevents differential deflection between the adjacent precast beams and also guarantees uniform distribution of live loads among the beams. TPT also helps in preventing the development of longitudinal cracks, which usually occurs along the joints between the precast units. If steel strands are used to apply the TPT forces, grouting must be used in the ducts to protect the steel strands. This hinders the ability to perform maintenance on the bridge. For instance, if a beam is damaged, the TPT cannot be removed in order to replace the damaged beam. Therefore, in a new approach which is followed by the Michigan Department of Transportation (MDOT), TPT strands are replaced with CFRP strands in order to avoid grouting of the ducts.

1.5 Fiber reinforced polymer (FRP) in bridge construction

1.5.1 Need for FRP reinforcement

The Prestressed Concrete Institute (PCI) design guidelines identify corrosion of steel reinforcement as one of three major and current problems in the nation's bridge inventory. Although concrete provides steel with an ideal alkaline environment for protection from atmospheric attack, corrosion of steel reinforcement remains a primary issue in reinforced and prestressed concrete structures. Corrosion of reinforcement occurs even if the concrete section is uncracked. Corrosion happens as a result of concrete carbonation or chloride ions penetration in processes called carbonation-induced corrosion or chloride-induced corrosion, respectively. Steel is thermodynamically unstable and it always tends to revert back to its original state whether it is steel oxide or steel hydroxide by reaction with oxygen and water.

Steel in an alkaline environment such as concrete creates an insoluble form of a thin passive protective layer at the surface of the reinforcement by combining the FE^{+} and the OH^{-} anions, which inhibits any corrosion. However, this passive protective coating is not stable in solutions containing chloride ions or where the PH is around 9 or less. On the other hand, concrete in nature is permeable and allows the ingress of water and chloride—from deicing chemicals. When the protective coating is broken, active corrosion of reinforcement occurs at a rate as high as several mm per year. The mechanics of chloride attack usually starts with the CL^{-} ions competing with the OH^{-} on the bond with FE^{+} and thereby attacking the passive protection film. In addition, the overall PH of the concrete is reduced, which accelerates the corrosion rate. The most detrimental consequence of chloride-induced reinforcement corrosion is the build-up of voluminous, insoluble corrosion products in the concrete. This leads to high internal stresses and eventually to cracking and spalling of the concrete cover (Hansson et al. 2007).

Carbonation of the concrete is another issue. Carbon dioxide from the atmosphere reacts with the calcium hydroxide and other hydroxides in the cement paste to form a neutralized solution around the steel in a chemical reaction such as [$Ca(OH)_2 + CO_2 \rightarrow CaCO_3 + H_2O$]. Carbonation starts at the surface of the concrete and can be detected by measuring the reduction in the PH at the surface. The PH on the surface can be 8 compared to 13 inside the concrete. The carbonation depth slowly increases with time until it reaches the reinforcement. Once the concrete around the reinforcement is neutralized, the protective coating of the steel is broken and corrosion starts at a

high rate. Unlike corrosion from chloride ions, corrosion due to carbonation is uniform and is extended over a wide area with no signs of spalling or concrete cracking at the earlier stages. However, rust stain may appear at the surface of the concrete as corrosion product dissolves in the water and migrates to the surface. Carbonation rate is usually at its maximum at moderate relative humidity (around 50 to 70 %). However, steel corrosion does not occur at that humidity range. Therefore, carbonation can be detrimental in the durability of concrete in hot climates where the concrete is easily dried out and periodically subjected to saturation by rainstorms. Chloride attack and carbonation can work together to induce a harsher scenario of steel corrosion and concrete deterioration (Hansson et al. 2007).

Several techniques were implemented in bridge construction to mitigate the problem of steel corrosion, which included providing adequate concrete cover, using epoxy coated reinforcement, or galvanizing the steel reinforcement. These corrosion-fighting techniques, though improve the durability of steel reinforcement, do not eliminate the corrosion problem. Sooner or later, steel reinforcement will undergo the process of corrosion, which imposes a threat to the structural element.

The recent development in the science of composite materials and their applications lured researchers and engineers to explore the option of replacing steel reinforcement with such non-corrosive materials. During the last few decades, extensive research efforts have be dedicated to evaluate the adequacy of replacing steel reinforcement with FRP materials in bridge construction. FRP is a composite material that is formed from an organic epoxy matrix reinforced with strong fibers such as glass, aramid, or carbon fibers and can be produced in different shapes such as bars, strands, wires, sheets, or plates. Depending on the strength of the epoxy matrix and the type of the reinforcing fibers, the overall physical and mechanical properties of FRP can be determined. For structural applications, carbon fiber reinforced polymer (CFRP) materials has favorable properties and better economic impact over both glass and aramid fiber reinforced polymer materials. CFRP is characterized by its exceptional high strength, high modulus of elasticity, and resistance to environmental conditions. Filaments of the carbon are produced by oxidation and heat pyrolysis of polyacrylonitrile (PAN) and recently from petroleum pitch delivered from oil processing. These fibers contain around 85 % carbon.

1.5.2 Recent field applications of FRP in bridge construction

FRP reinforcement has been successfully employed in several bridge construction projects all over the world and currently, there are various manufacturers fulfilling the need of the global market with FRP materials. In Japan, for instance, the production of FRP materials has shown significant increase since the 1990s with seven groups of FRP producers, construction, and design firms. Table 1.5-1 shows some of the companies and their products in civil engineering applications, while Table 1.5-2, 3, 4, and 5 show a few of the field applications of FRP materials in the bridge industry in Canada, Japan, USA, and Europe, respectively.

Table 1.5-1 FRP manufacturers and main products

Manufacturer	Country	Product
CFCC Group (Tokyo Rope Mfg. Co. Ltd.)	Japan	Carbon fibre cables and bars
Arapree Group (Nippon Aramid Co., Ltd. And Kajima Corp.)	Japan	Aramid prestressing elements
Technora Group (Teijin, Ltd., and Sumitomo Construction Co., Ltd)	Japan	Aramid bars/cables
Fibra Group (Shinko Wire Co., Ltd)	Japan	Woven bars and cables (Aramid)
Leadline group (Mitsubishi Chemical Co.)	Japan	Carbon fibre bars and cables
NACC Group (Nippon Steel Corp., Suzuki Metal Industry Co., Ltd)	Japan	Carbon fibre cables
NEFMAC group (Shimizu Corp.)	Japan	Mesh reinforcement
Marshal Composite Technologies LCC	USA	C-Bar

Table 1.5-2 Reinforced or prestressed FRP bridges in Canada

Bridge	Province	Year	System	FRP Component
Beddington Trail Bridge	Alberta	1993	CFCC Leadline	Prestressing of main beams (first application)
Catham Bridge	Ontario	1996	NEFMAC nets (carbon)	Slab cantilevers
Joffre Bridge	Quebec	1997	C-bar carbon	Slab reinforcement (partially)
Taylor Bridge	Manitoba	1997	CFCC, Leadline, C-bar (glass)	Prestressing of main beams, slabs and stirrup reinfocement, connections to guide rails
Crowchild Trail Bridge	Alberta	1997	C-bar glass	Slab reinfocement over columns and for canilevers
Bishop Grandin Boulevard	Manitoba	1998	GFRP dowels	Bridge deck joints

Table 1.5-3 Reinforced or prestressed FRP bridges in Japan

Bridge	Location	Year	System	FRP Component
Shinmiya Bridge	Ishikawa	1988	CFCC	Prestressing of main beams
Birdie Bridge	Ibaraki	1989	CFCC, Arapree, Leadline	Formwork elements, prestressing or ribbon, ground anchors
Bachiawa Minami Bridge	Fukuoka	1989	Leadline	Prestressing of main beams
Sumitomo Bridge (1)	Tochigi	1989	Technora	Prestressing of main beams, transverse prestressing
Talbus Bridge	Tochigi	1990	FiBRA	Prestressing of beams
Sumitomo Bridge (2)	Tochigi	1991	Technora	Prestressing of main beams
Hishinegawa Bridge	Ishikawa	1992	CFCC	Prestressing of main beams, stirrup reinforcement
Hisho Bridge	Aichi	1993	CFCC	Prestressing of main beams
Yamanaka Bridge	Tochigi	1996	FiBRA	Prestressing of main beams
Stress Ribbon Bridge	Nagasaki	1993	FiBRA	Prestressing of ribbon
Rainbow Bridge	Tokyo	1993	FiBRA	Prestressing of slabs
Mukai Bridge	Ishikawa	1995	CFCC	Prestressing of main beams

Table 1.5-4 Reinforced or prestressed FRP bridges in USA

Bridge	State	Year	System	FRP Component
McKinleyville Bridge	West Virginia	1996	C-Bar	Bridge deck, first use of reinforcing bars in the USA
Kentucky Boubon County Bridge	Kentucky	1997	C-Bar	Bridge deck
Route 668 Bridge over Gills creek	West Virginia	2003	GFRP	Bridge deck
Salem Ave. Bridge	Ohio	1999	GFRP	Bridge deck
Sierrita de la Cruz Creek Bridge	Texas	2001	GFRP	Bridge deck
53rd Avenue Bridge	Iowa	2001	GFRP	Bridge deck
Bridge Street Bridge	Michigan	2001	CFCC, Leadline	Bridge deck, first use of FRP prestressing
Penobscot Narrows Cable Stayed Bridge	Maine	2007	CFCC	Cable stayed system

Table 1.5-5 Reinforced or prestressed FRP bridges in Europe

Bridge	Country	Year	System	FRP Component
Lunen's Gasse Bridge Dusseldorf	Germany	1980	Polystal (12 cables each with 19 bars)	Slab prestressing
Ulenbergstrasse Bridge Dusseldorf	Germany	1986	Polystal (59 cables each with 19 bars)	Parabolic slab prestressing, degree of prestress 50%
Marienfelde Bridge Berlin	Germany	1988	Polystal (7 cables each with 19 bars)	External prestressing
Schiessbergstrasse Bridge Leverkusen	Germany	1991	Polystal (27 cables each with 19 bars)	Parabolic slab prestressing, degree of prestress 50%
Oststrasse Bridge	Germany	1991	CFCC	Prestressing of main beams
Notsch Bridge Karnten	Austria	1992	Polystal (41 cables each with 19 bars)	Slab prestressing
Fidgett's Bridge	England	1995	Eurocrete glass fibre bars	Slab reinforcement
Oppengaard Bridge	Norway	1996	Eurocrete glass fibre bars, Parafil cables	Slab reinforcement ties
Herning Bridge	Denmark	1999	CFCC	Stay cables, slab prestressing, slab reinforcement

1.5.3 Experimental investigations in CFRP reinforcement

Grace et al. (1999) developed a technology to combine bonded internal CFRP tendons with unbonded externally draped CFRP tendons in bridge construction. This technology was successfully implemented in the construction of Bridge Street Bridge, the first bridge built in the United States with CFRP as the main reinforcement (Grace et al. 2002). The design, fabrication, erection, long-term monitoring program, and load-distribution behavior of this concrete bridge was presented by Grace et al. (2003 and 2005).

Grace et al. (2003) presented the response of a newly developed two-span continuous double T bridge system with internal and external prestressing using CFRP leadline tendons. The effect of pre- and post-tensioning on the overall strain distribution was examined by first subjecting the bridge to 15 million cycles of repeated load at a constant amplitude equal to the service load, and then by loading the bridge to failure.

Fam et al. (1997) conducted reduced scale tests on beams constructed to represent the beams of Taylor Bridge in Manitoba, Canada. Two types of CFRP reinforcements for shear and prestressing were provided in the 30.5 ft long I-girders, which were compared to similar girders

with conventional steel strands and stirrups. Various web reinforcement ratios were used for each type of CFRP reinforcements. Steel and CFRP beams showed similar flexural behavior from zero loading to cracking. In the post-cracking stage, the CFRP beams showed nearly linear load-deflection relationship until failure while steel beams showed ductile behavior near failure. The effect of the CFRP stirrup configuration and size on the shear behavior and their performance in providing the dowel action between the girder and top slab was also analyzed.

Abdelrahman and Rizkalla (1999) investigated the flexural performance of beams partially prestressed with CFRP tendons. The focus of the investigation was on prestressing ratio and degree of prestressing. Eight specimens were prestressed with CFRP (Leadline) tendons and two specimens were prestressed with steel strands (control specimens). The CFRP tendons had a modulus of elasticity of 21,300 ksi, ultimate strength of 285 ksi, and a corresponding ultimate strain of 1.3 %. Horizontal cracks at the level of prestressing reinforcement were observed at failure. These cracks were attributed to the release of elastic strain energy when the bars ruptured. Traditionally, with steel reinforcement, under-reinforced beams yield more deflection than over-reinforced beams. However, this study showed that the maximum deflection of specimens which failed by bar rupture (under-reinforced) was less than the maximum deflection of the specimens which failed due to concrete crushing. In addition, beams prestressed with CFRP tendons had less cracks than beams prestressed with conventional steel strands due to a lower flexural rigidity. However, the average crack widths of the beams reinforced with CFRP tendons were larger. Overall, it was observed that specimens prestressed with CFRP tendons were significantly affected by the level of prestress. A higher level of prestress resulted in higher breaking load and a lower corresponding deflection.

Abdel-Rahman and Rizkalla (1999) proposed partial prestressing at low-jacking stresses to design concrete members prestressed with CFRP reinforcement. This technique is capable of reducing the cost and improving deformability by changing parameters such as prestressing ratio, level of prestressing, and distribution of the CFRP bars in the tension zone.

The arrangement of vertical reinforcement across the depth is a critical factor in flexural capacity, particularly in AASHTO beams and T beams. To maximize eccentricity which inherently increases the flexural capacity of the beam, it is advantageous to locate the prestressing

tendons as far from the neutral axis of the beam as possible. In decked bulb T sections, the designer should locate the longitudinal reinforcement based on strength requirements.

Progressive tendon fracture may occur in FRP prestressed concrete beams when tendons are vertically distributed throughout the section (Dolan and Swanson 2002). When straight prestressing tendons are distributed vertically throughout the section, the tendons farthest from the neutral axis are subjected to the highest strain. In conventional steel reinforced prestressed sections, the layer farthest from the neutral axis yields first. However, the strands do not rupture and the beam continues to sustain the applied loads. When the extreme layers of FRP strands reach the ultimate strain capacity, the strands rupture and the load carrying capacity of the beam is reached. As a result, the strength requirements for steel prestressed beams are not valid for under-reinforced FRP prestressed beams.

Naaman et al. (1993) experimentally and theoretically investigated partially prestressed concrete T beams with carbon fiber composite strands. Progressive failure was achieved in a T beam reinforced with 2#4 Grade 60 steel bars in the bottom layer, two non-prestressing carbon fiber composite cable (CFCC) seven-wire strands just above the steel bars, and two CFCC prestressing strands (1×7) directly above the CFCC non-prestressing strands. The post-peak load-deflection behavior was characterized by step-like decrease corresponding to the rupture of CFCC tendons.

Morais and Burgoyene (2003) proposed step layering of FRP reinforcement to develop a progressive failure and to improve ductility. However, the ultimate load capacity of the beam is achieved once and cannot be maintained after the first failure. Therefore, under real loading applications, the beam will initially fail unless the load can be distributed to other structural elements away from the failed beam. In the case of under-reinforced FRP sections, ACI 440.1R-06 guidelines suggest reserving strength in the FRP members to compensate for the lack of ductility. Otherwise, the FRP flexural elements shall be designed as over-reinforced. Various studies show that over-reinforced FRP beams exhibit a moderate amount of ductility before crushing of the concrete.

Ductility is the ability of a structure to sustain inelastic deformation without reduction in its load-carrying capacity prior to failure. Grace et al. (1998) proposed a new methodology to evaluate ductility of CFRP prestressed beams and bridges with both rectangular and skewed geometries. It

was observed that the CFRP reinforced bridges exhibited a reasonable amount of absorbed energy. Several loading/unloading cycles were applied to the bridge model to separate the elastic energy from the inelastic energy. The elastic energy ($E_{elastic}$), inelastic energy ($E_{inelastic}$), and additional inelastic energy ($E_{inelastic,addl}$) were quantified from the load-deflection response. The ductility was represented by the energy ratio. The energy ratio was defined as the ratio of absorbed inelastic energy to total energy, where the total energy was the summation of the elastic and the inelastic energies (Grace et al. 1998). The energy ratio can be expressed as:

$$\text{Energy ratio} = \frac{E_{inelastic}}{E_{Total}} = \frac{E_{inelastic}}{E_{elastic} + E_{inelastic} + E_{inelastic,addl}}$$

The failure mode of a bridge can be classified as ductile for energy ratios greater than 75 %, semi-ductile for energy ratios between 70 and 74 %, and brittle for energy ratios less than 69 %.

Jo et al. (2004) evaluated ductility of concrete beams prestressed with CFRP tendons. The ductility index was expressed as the ratio of the elastic energy at failure to the total energy of the beam. It was reported that concrete beams prestressed with CFRP tendons had sufficient ductility when compression failure took place by crushing of concrete or when unbonded tendons were used. To achieve increased ductility, a compression-controlled failure and unbonded tendons were recommended for CFRP reinforced beams.

Mutsuyoshi et al. (1993) put forth a strategy to improve ductility of prestressed concrete members reinforced with FRP tendons by improving the quality of the concrete. It was confirmed that compressive stress-strain behavior of confined concrete greatly improved the ductility.

Hassan et al. (1999) performed experimental investigations on full-scale models representing a portion of a highway bridge slab reinforced with CFRP and GFRP reinforcement. The static load-deflection behavior, crack patterns, strain distribution, and failure mode were reported and compared with the results obtained from nonlinear finite element analysis. Numerical models were generated and used to examine the influence of various parameters including the type of reinforcement, boundary conditions, and reinforcement ratio. Recommendations were made for CFRP and GFRP reinforcement based on the strength and serviceability results. Stroll et al. (2000) designed, fabricated, and tested two full-scale high-strength concrete bridge beams reinforced with FRP products for prestressing and shear reinforcement.

Abdel-Rahman and Rizkalla (1999) proposed a simplified method to calculate the deflection of beams prestressed with CFRP reinforcement under short-term and repeated loading. Throughout the experimental program, bond factors were introduced to account for tension stiffening of concrete beams prestressed with CFRP tendons and to determine the location of the neutral axis of cracked prestressed sections. Design guidelines were proposed to predict the deflection of beams partially prestressed with CFRP reinforcement.

El-Sayed et al. (2006) reported experimental data on the flexural performance and shear strength of high-strength concrete slender beams reinforced with FRP bars and conventional steel reinforcement. The authors conducted shear tests on large-scale reinforced concrete beams without stirrups using high-strength and normal-strength concrete with varying reinforcement ratios and modulus of elasticity of the longitudinal reinforcing bars. The experimental shear strengths of the FRP (carbon and glass) and steel reinforced concrete beams were compared to theoretical predictions provided by ACI 440.1R-03. It was concluded that the high-strength concrete beams exhibited slightly lower relative shear strength when compared to normal-strength concrete beams. The predicted shear strengths using ACI 440.1R-03 were found to be conservative.

Zou and Shang (2007) investigated the long term performance of FRP prestressed beams. The long term effects on curvature, deflection, strains, cracking, loss of prestress, and transfer length of FRP were all investigated. The experimental investigations also addressed the level of prestressing force, the level of sustained service loading, and concrete strength. The results showed that the creep of the CFRP was less than 0.2 %. In addition, the transfer length ranged from 11 to 31 in. It was concluded that the strength of the concrete at transfer was one of the major factors affecting the transfer length of the CFRP. A factor accounting for the concrete strength was proposed for estimating the transfer length of the CFRP tendons. Despite the creep and shrinkage of concrete and the relaxation of the tendon itself, the range for transfer length did not vary with time. It was also concluded that the performance of concrete beams prestressed with CFRP tendons meets the serviceability criteria in terms of deflection and cracking. The long-term performance was comparable to the performance of beams prestressed with steel tendons. Serviceability performance was improved with an increase in the concrete strength. The researchers defined a deformability index for prestressed concrete beams in terms of deflection and strength factors. The deflection factor represented the ratio of the deflection at failure to the deflection at first cracking,

while the strength factor represented the ratio of the ultimate moment (or load) to the cracking moment (or load).

1.5.4 Analytical representation for design of FRP sections

Grace et al. (1999) developed a mathematical solution for CFRP prestressed concrete skew bridges based on a closed-form series function. The bridge was assumed to behave as an orthotropic plate and membrane theory was used to simulate the effect of internal and external prestressing forces in the longitudinal and transverse directions. Flexural and torsional rigidity formulae were derived and implemented in the solution to determine deflections, induced stresses, and strains during various stages of construction. The results were validated by experimental results and finite element analysis using ABAQUS. The results of the mathematical solution matched the results of the experimental investigations and the results of the finite element analysis which validated the proposed rigidity formulae and the developed mathematical solution.

Grace and Abdel-Sayed (1999) experimentally investigated the design and construction techniques of CFRP prestressed concrete skew bridges. The results indicated that the repeated load has no adverse effect on the dynamic and static characteristics of CFRP reinforced skew bridges and had an insignificant effect on the load-distribution in the transverse direction. All the externally draped prestressing tendons remained intact under repeated and ultimate loads. The transverse load-distribution exhibited the same characteristics for bonded and unbonded transverse post-tensioning tendons.

Grace and Singh (2003) introduced a combined design approach based on strain compatibility for beams prestressed with bonded prestressing and unbonded post-tensioning CFRP tendons arranged in multiple vertical layers. The authors stated that this approach is applicable to various beam cross sections such as double T, box, or AASHTO I beam sections (Figure 1.5-1). The failure mode was determined by comparing actual reinforcement ratio (ρ_f) with the balanced reinforcement ratio (ρ_{fb}). The actual reinforcement ratio is obtained from the equilibrium of forces and compatibility of strains in the cross-section. The balanced reinforcement ratio and the actual reinforcement ratio can be calculated as follows:

$$\rho_{fb} = 0.85\beta_1 \frac{f_c^{'}}{f_{fu}} \frac{\varepsilon_{cu}}{\varepsilon_{cu} + \varepsilon_{fu} - \varepsilon_{pbmi}}$$

$$\rho_f = \frac{\sum_{j=1}^{m} F_{pi} + f_{pbb}A_{pb} + f_{pnbb}A_{pn} + F_{pui} + f_{pub}A_{fu} - f_{pnfb}A_{pnf}}{bd_m f_{fu}}$$

Where:

β_1 Depth of an equivalent rectangular stress block divided by the distance from the extreme compression fiber to the neutral axis (ACI-318 2005)

$f_c^{'}$ Specified compressive strength of the concrete

f_{fu} Specified tensile strength of bonded prestressing tendons

ε_{pbmi} Initial prestressing strain in bonded tendons

A_{pb} Total cross-sectional area of bonded tendons

A_{pn} Total cross-sectional area of non-prestressing rods

A_{fu} Total cross-sectional area of unbonded tendons

A_{pnf} Total cross-sectional area of non-prestressing rods located in the compression flange

F_{pi} Incremental initial jacking pretensioning force

F_{pui} Total initial post-tensioning force

f_{pbb} Flexural stress in the equivalent bonded tendon at the balanced condition

f_{pnbb} Flexural stress in equivalent non-prestressing tendon at the balanced condition

f_{pub} Flexural stress in equivalent unbonded tendons at the balanced condition

f_{pnfb} Flexural stress in equivalent non-prestressing tendon located in the compression flange at the balanced condition

b Flange width of the beam

d_m Distance from centroid of the bottom prestressing tendons to extreme compression fibers

Recently, Youakim et al. (2007) introduced a simple method to calculate the long-term prestress loss and change in concrete stresses in continuous prestressed concrete members with either CFRP tendons. The authors concluded that the prestress loss in FRP tendons was significantly less than that of steel strands. This was primarily due to the lower modulus of elasticity of FRP tendons. The long-term change in concrete stresses and deflection could either be smaller or greater than those of comparable girders prestressed with steel tendons. This is dependent on the type of FRP tendons and the initial stress profile of the cross-section under consideration.

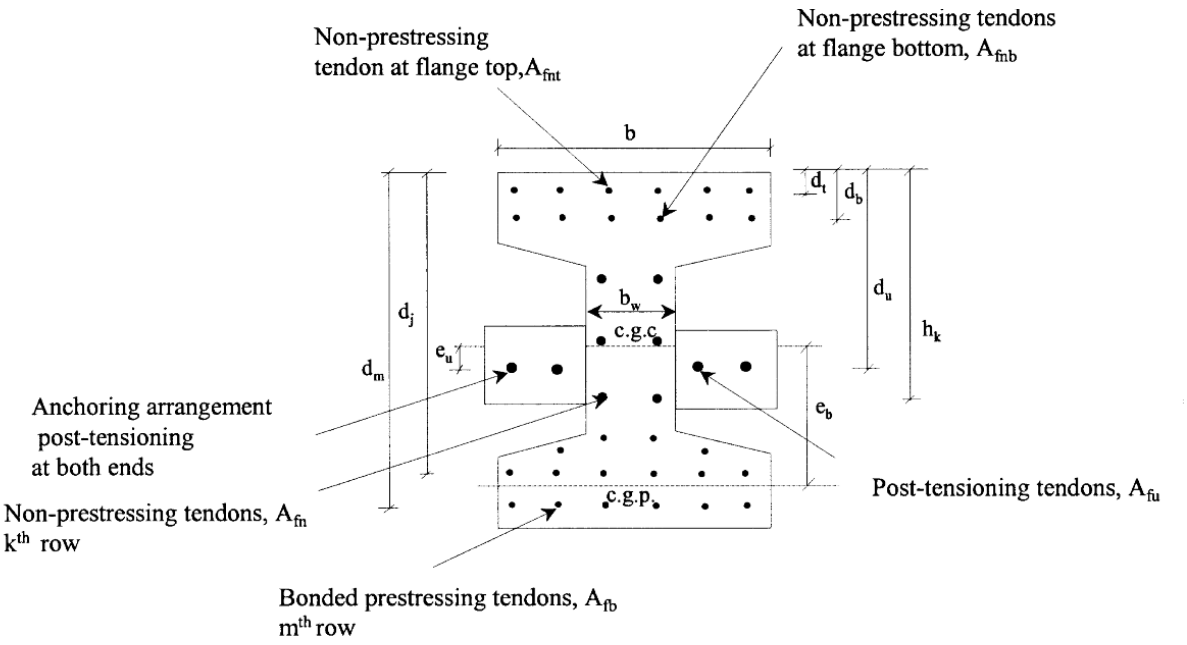

Figure 1.5-1 Typical AASHTO beam section used for design approach (Grace and Singh 2003)

In summary, it was concluded that while FRP reinforced/prestressed beams may not exhibit the same amount of ductility exhibited by steel beams, there are different warning signs such as excessive deflection and dense crack pattern that can serve as a clear visual warning sign before failure. In addition, concrete crushing is marginally more desirable than the rupture of FRP reinforcement because of the pseudo-plastic behavior of concrete members before rupture. However, both failure modes are acceptable in governing the flexural design of FRP reinforced/prestressed concrete members as long as strength and serviceability criteria are satisfied.

1.6 Skew angle in bridges

Bridges have to overcome natural obstacles such as rivers and mountain terrains along with manmade obstacles such as complex intersections (Huang et al. 2004). Therefore, bridges are often skewed to overcome these obstacles. Ebeido and Kennedy (1996) experimentally investigated the effect of the skew angle on the applied moment and moment-distribution factors. The experimental program included the construction and experimental testing of three I-beam bridges models. One bridge model had no skew and two bridge models had a skew angle of 45°. In addition, a parallel finite element analysis using ABAQUS was conducted to evaluate different span lengths in skewed bridge models. It was observed that the beam moment reduced due to the effect of the skew angle. It was also observed that skew angles less than 30° had an insignificant effect on the moment-distribution factor whereas skew angles more than 30° increased the moment-distribution factor (Figure 1.6-1).

Khaloo and Mirzabozorg (2003) conducted a finite element study on load-distribution factors in skewed bridges. The bridge models were examined with; no transverse diaphragms, transverse diaphragms parallel to the support, and transverse diaphragms perpendicular to the longitudinal beams. These diaphragm arrangements were analyzed under skew angles of 0°, 30°, 45°, and 60°. The authors noted that transverse diaphragms parallel to the support yielded the lowest load-distribution factor in skew bridges. The authors also indicated that AASHTO calculations of load-distribution factors are conservative.

Badwan and Liang (2007) performed a grid analysis to determine an optimum post-tensioning stress for a multi-beam deck. The effect of different skew angles on the transverse post-tensioning stresses was also studied in detail. The study revealed that skew angles more than 30° has a significant effect on post-tensioning stresses. The study also showed that AASHTO specifications are adequate or conservative for highly skewed bridges.

Several other investigations (Khaloo and Mirzabozorg 2003) were conducted to evaluate the distribution of truck wheel loads on multi-beam bridges. The wheel loads were placed at various locations on the bridge. The investigations addressed the performance of various beam connections including grouted shear keys and welded steel connectors and extended to include the effect of different diaphragm arrangements, transverse post-tensioning levels, girder spacing, and skew

angles. Findings of the research showed that transverse diaphragms were effective in distributing live loads on bridges.

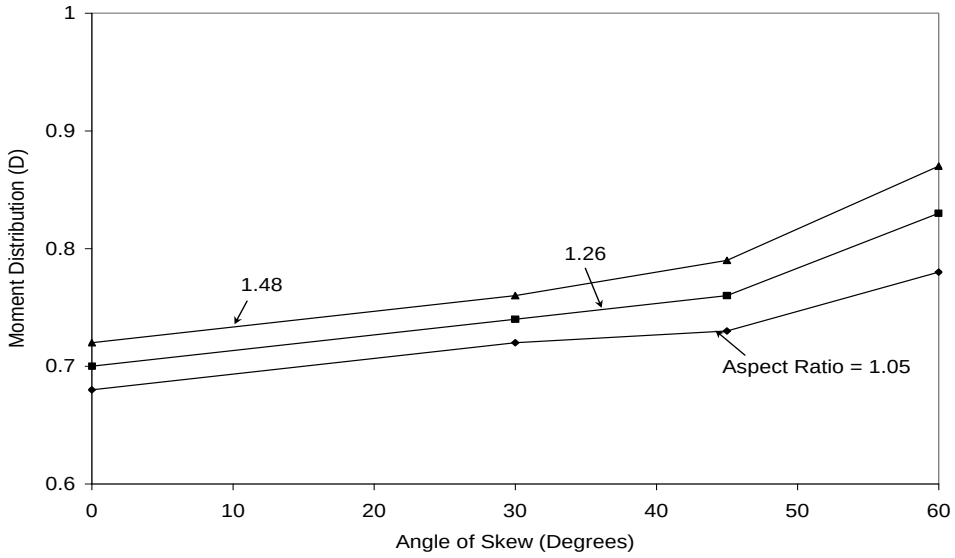

Figure 1.6-1 Effect of skew angle on the moment-distribution factor for an external girder (Ebeido and Kennedy 1996)

CHAPTER 2: EXPERIMENTAL INVESTIGATION

2.1 Introduction

An experimental investigation was initiated and executed to validate the performance of decked bulb T beam bridge system with CFCC reinforcement and to address all underlying technical and construction issues. The experimental investigation included the construction and testing of five one-half-scale control decked bulb T beams in addition to a complete one-half-scale bridge model. The bridge model consisted of five decked bulb T beams connected together with UHPC shear key joints and seven equally-spaced transverse diaphragms. The control beams and the bridge model had a total length of 41 ft, an effective span of 40 ft, a depth of 16 in., and initial prestressing force of 132 kip/beam. One control beam was tested to failure under shear loading and four beams were tested to failure under flexural loading. On the other hand, the bridge model was exposed to different loading configurations through three states: service limit state, where the applied load was not enough to induce flexural cracks, post-cracking limit state, where the applied load was larger than the cracking load of the bridge model, and strength limit state, where the load was applied to induce failure of the bridge. The following sections provide the details of specimens, sequence of construction, order of testing, observed performance and failure modes, and the main outcomes of the experimental investigation.

2.2 Details of control beams

The control beams (Figure 2.2-1) were identical in cross section dimensions with a top flange width of 18 in., a depth of 16 in. and a bottom flange width of 12 in., but varied in the reinforcement configuration. A summary of the reinforcement is shown in Table 2.2-1, where the acronym of the beams is composed of four letters. The first letter refers to the type of longitudinal reinforcement (S for steel and C for CFCC). The second letter refers to the type of transverse reinforcement (S for steel stirrups and C for CFCC stirrups). The third letter refers to the type of loading (F for flexural loading and S for shear loading). The last letter refer to the reinforcement ratio (U for under-reinforced section, B for balanced section, and O for over-reinforced section). As shown in the table, four beams including one beam with steel reinforcement were tested under flexural loading, while the fifth beam was provided with CFCC stirrups and was tested under shear loading.

Table 2.2-1 Details of reinforcement in control beams

	Longitudinal Reinforcement	Transverse reinforcement	Type of loading	Reinforcement ratio (Anticipated failure mode)
S-S-F-U	Steel	Steel	Flexural	Under reinforced (Steel yield, tension failure)
C-S-F-U	CFCC	Steel	Flexural	Under reinforced (CFCC rupture, tension failure)
C-S-F-B	CFCC	Steel	Flexural	Balanced reinforcement (Conc. Crushing & CFCC rupture)
C-S-F-O	CFCC	Steel	Flexural	Over-reinforced (Conc. crushing, compression failure)
C-C-S-B	CFCC	CFCC	Shear	Balanced reinforcement (concrete web crushing, shear failure)

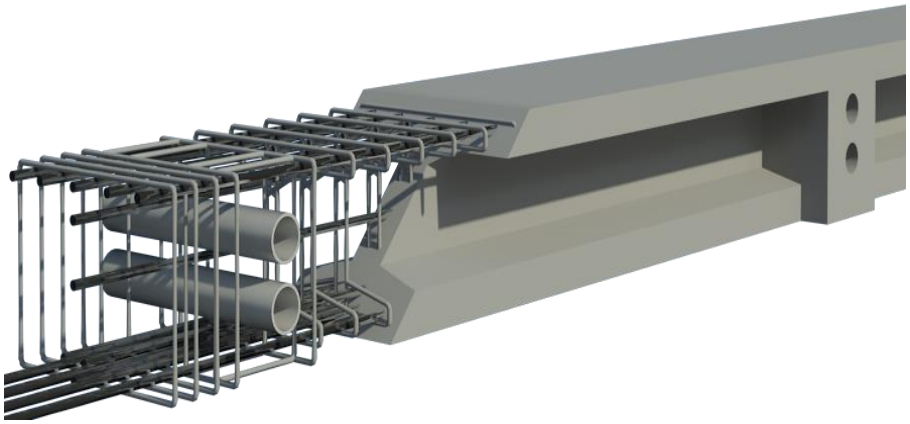

Figure 2.2-1 Configuration of control beams

As shown in Figure 2.2-2, Beam S-S-F-U was prestressed with four 7-wire low-relaxation steel strands with a diameter of 0.6 in. Each strand was prestressed with an initial prestressing force of 33 kip. In addition, three No. 5 Grade 60 steel deformed bars were provided as additional non-prestressed bottom reinforcement. The top flange was reinforced with five deformed steel bars No. 5 and two additional No. 5 bars were provided through the depth of the beam. In the transverse direction, the beam was provided with No. 3 steel stirrups with a center-to-center spacing of 4 in.

Beam C-S-F-U, shown in Figure 2.2-3, was prestressed with four steel strands with a diameter of 0.6 in. Similar to beam S-S-F-U, each strand was prestressed with an initial prestressing force of 33 kip. No non-prestressed reinfrocement was provided at the bottom flange. The reinformecent

of the top flange and the web was similar to other control beams where five non-prestressed CFCC strands with a diamter of 0.6 in. were provided as top flange reinforcement and two strands of the same diameter were provided in as web reinforcement.

Designed with a balanced reinforcement ratio, Beam C-S-F-B, shown in Figure 2.2-4, contained the same reinforcement as beam C-S-F-U with the exception that three additional non-prestressed steel strands with a diamter of 0.6 in. were provided at the bottom flange to increase the reinforcement ratio and approach the balanced failure. On the other hand, to satisfy the requirement for an over-reinforced section, Beam C-S-F-O, shown in Figure 2.2-5, included five non-prestressed strands in addition to the original four prestressed strands in the bottom flange. The physical and mechanical properties of all reinforcement are given in Table 2.2-1. During the course of the study, the research team received two lots of CFCC (Lot #1 and 2, shown in the table) strands with a slight difference in the ultimate strength, strain, and elastic modulus.

While all previously mentioned beams were reinforced with steel stirrups, the fifth beam, Beam C-C-S-B, was reinforced with CFCC stirrups with a diameter of 0.4 in. and a center-to-center spacing of 4 in. As shown in Figure 2.2-6, this beam was reinforced in the longitudinal direction with four prestressed CFCC strands and three non-prestressed CFCC strands, which is similar to the reinforcement of Beam C-S-F-B. This amount of reinforcement would achieve the balanced failure for this section.

Table 2.2-2 Physical and mechanical properties of reinforcement

	Diameter (in.)	Area ($in.^2$)	Yield strength (ksi)	Ultimate strength (ksi)	Elastic modulus (ksi)	Failure strain (%)
CFCC strands, Lot #1	0.60	0.179	-	375	23,061	1.6
CFCC strands, Lot #2	0.60	0.179	-	380	22,916	1.7
CFCC stirrups	0.44	0.090	-	384	22,625	1.7
CFCC (TPT)	1.00	0.472	-	384	22,625	1.7
Steel strands	0.60	0.217	230	279	28,400	5.4
Steel deformed bars	0.63	0.301	60	90	29,000	5.0
Steel stirrups	0.38	0.110	60	90	29,000	5.0

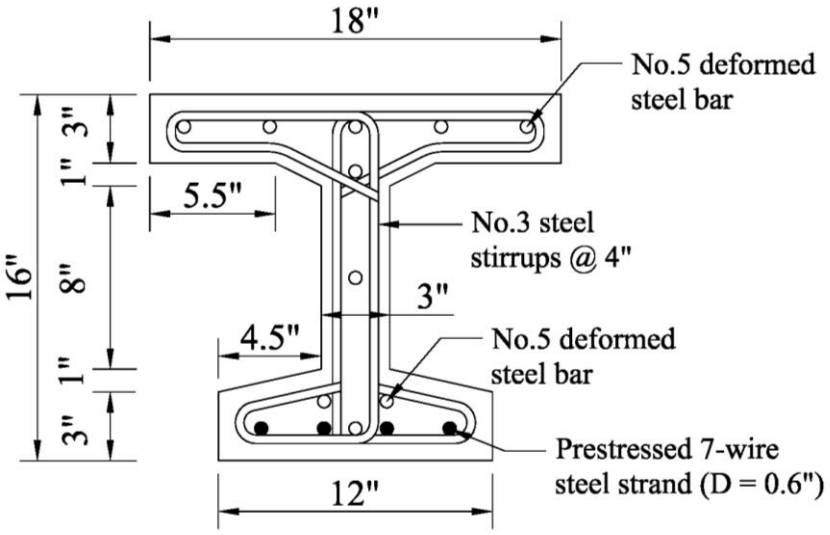

Figure 2.2-2 Details of Beam S-S-F-U

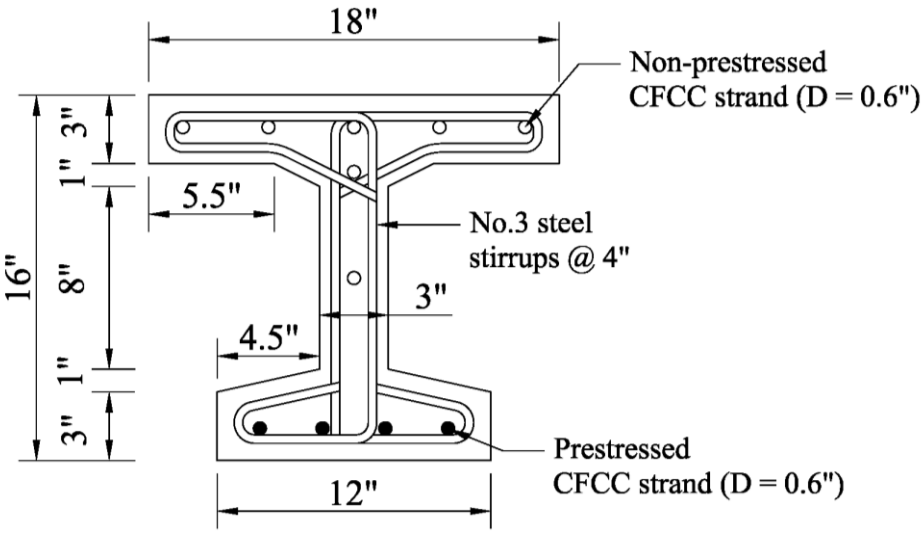

Figure 2.2-3 Details of Beam C-S-F-U

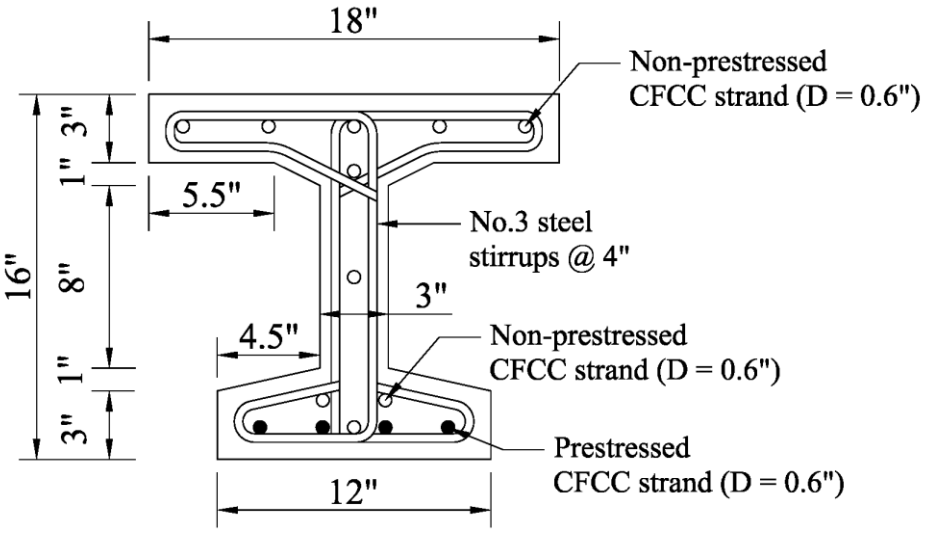

Figure 2.2-4 Details of Beam C-S-F-B

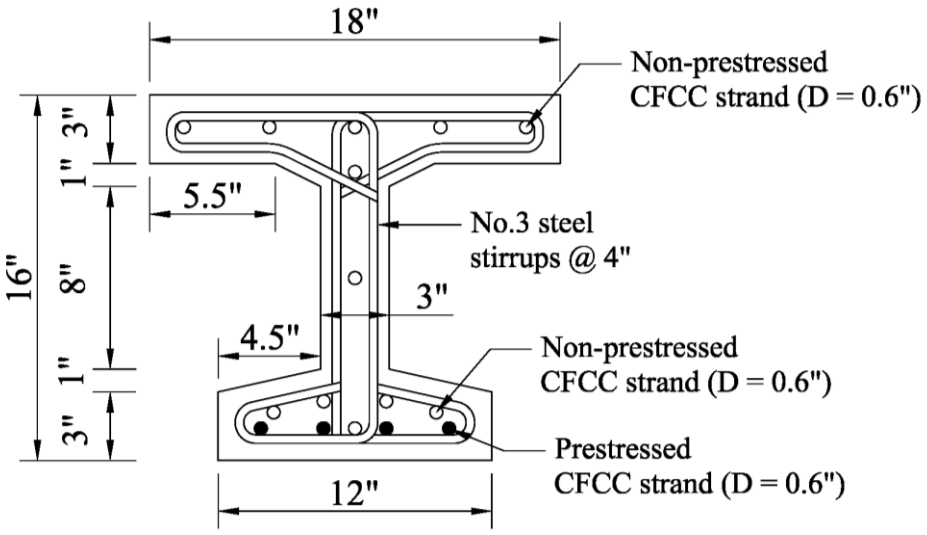

Figure 2.2-5 Details of Beam C-S-F-O

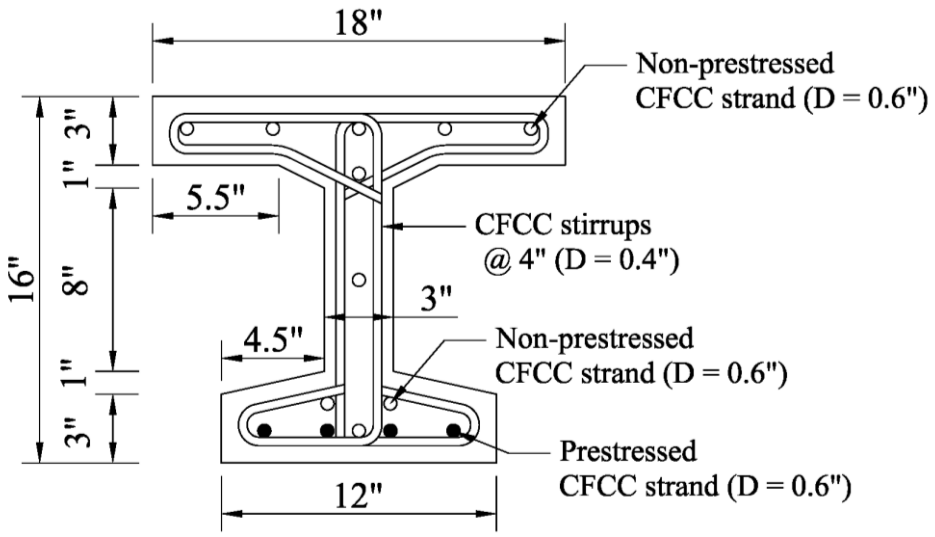

Figure 2.2-6 Details of Beam C-C-S-B

2.3 Details of bridge model

The bridge model consisted of five decked bulb T beams (Figure 2.3-1 and Figure 2.3-2). The beams were interconnected at their top flanges using UHPC shear key joints. In addition, seven full-depth equally spaced transverse diaphragms were provided through the span of the bridge model. Each diaphragm was provided with two 3.0-in. conduits to accommodate two transverse post-tensioning strands. The bridge model was simply supported over an effective span of 40 ft and had a total deck width of 8.5 ft. The reinforcement and prestressing of each beam was similar to those of Beam C-S-F-B. In addition, the transverse post-tensioning system consisted of a total of 14 CFCC strands with a diameter of 1.0 in. (two strands per diaphragm). Each strand was provided with two anchorage devices at its ends. The anchorage device consisted of a stainless steel threaded sleeve and a stainless steel locking nut. The anchorage was attached to the strand using highly expansive grout material (HEM).

The stirrups in the beams protruded for a distance of 3.0 in. from the side of the top flange to form the reinforcement for the shear key joints. Similarly, the transverse reinforcement of the diaphragms extended beyond the concrete surface and was spliced using additional reinforcement crossing the space between the beams.

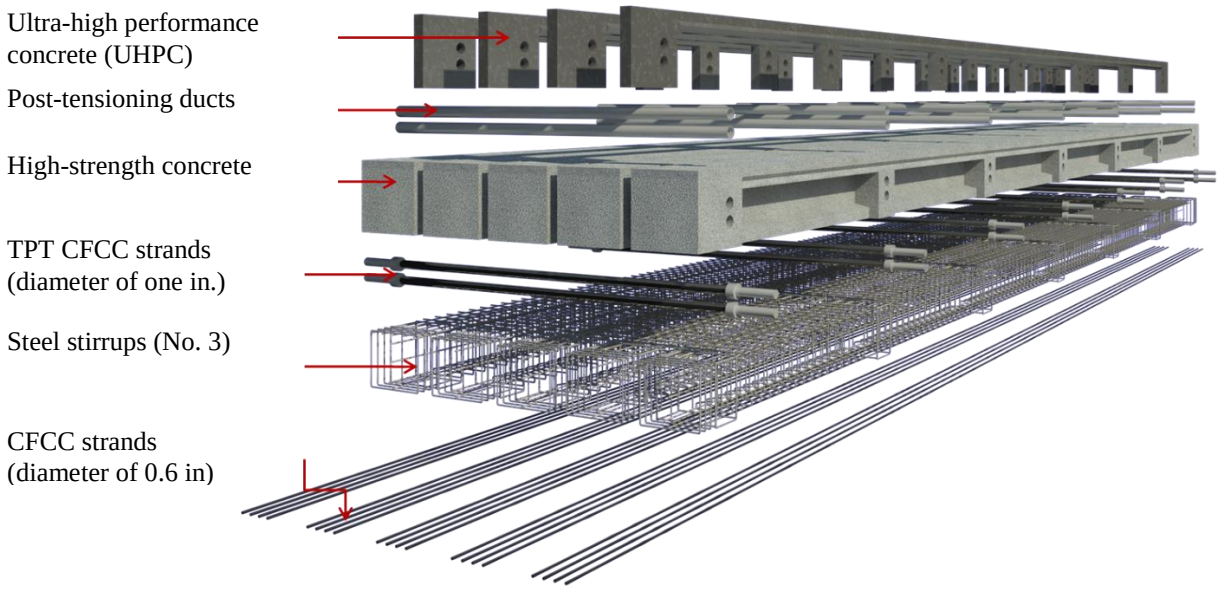

Figure 2.3-1 Components of bridge model

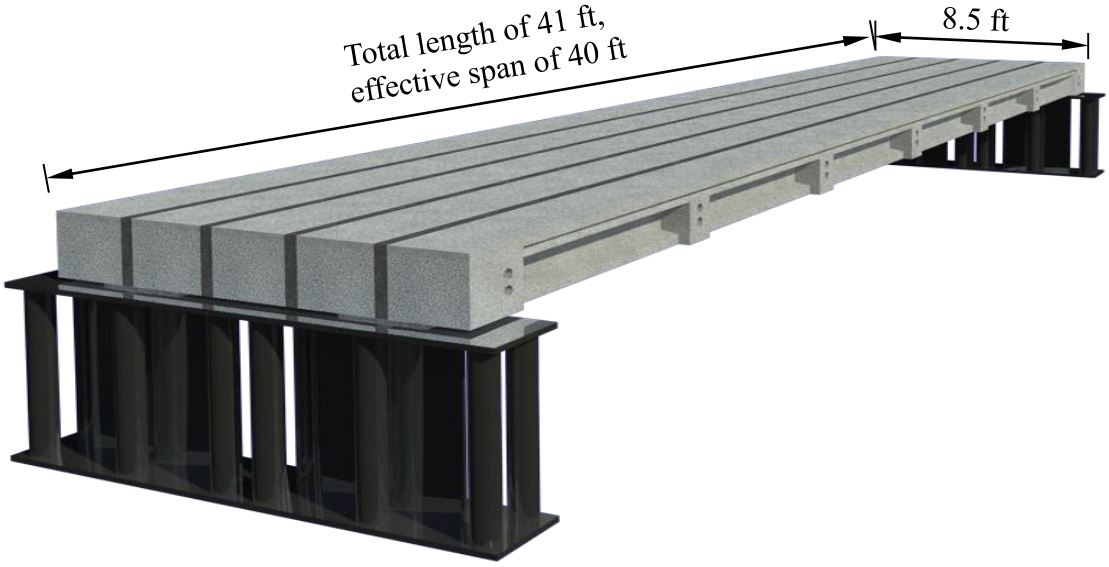

Figure 2.3-2 Layout of the bridge model

2.4 Details of construction of control beams

2.4.1 Construction & testing facility

The construction and testing of the specimens took place inside the structural engineering research facilities at Lawrence Technological University. The research facilities includes the Center for Innovative Materials Research (CIMR) and the Structural Testing Center (STC).

2.4.1.1 Center of Innovative Material Research (CIMR)

CIMR, Figure 2.4-1, is a 7,000 square feet testing facility that is equipped with a full-scale testing frame, two 330,000 lb pre-tensioning beds, an environmental/loading chamber with a testing frame, and a fire/loading chamber with a testing frame. The full-scale testing frame in CIMR has plan dimensions of 52 ft x 17 ft and is composed of three bays, each supporting a 250,000 lb MTS hydraulic testing actuator. With this particular testing facility, the research team was capable of testing the control beams and the bridge model as it can host specimens of spans up to 100 ft and widths up to 12 ft. The pre-tensioning beds are capable of supporting the prestressing forces for pre-tensioned beam specimens of spans up to 61 feet. Figure 2.4-1 shows the testing frame (1) and one of the pre-tensioning beds (2).

Figure 2.4-1 Center of Innovative Materials Research (CIMR).

2.4.1.2 Structural Testing Center (STC)

The Structural Testing Center (STC) contains two testing frames that are used to induce service and strength load conditions to bridge beams. One frame, (Figure 2.4-2), supports two 150,000-lb MTS hydraulic testing actuators. The other frame supports two 100,000-lb MTS hydraulic testing actuators. Two 300,000-lb prestressing beds which are approximately 61 ft. long are used for the production of various prestressing beams. The STC was also used to conduct the current investigation. The loading frame (1) in Figure 2.4-2 was used to test four control beams. The pretensioning bed (2) in Figure 2.4-2 was used during the construction and prestressing of the control and the bridge beams. The prestressing bed is composed of 8-ft-deep reinforced concrete bed with two steel bulk heads (3) secured to the concrete foundation using high-strength anchorage bolts.

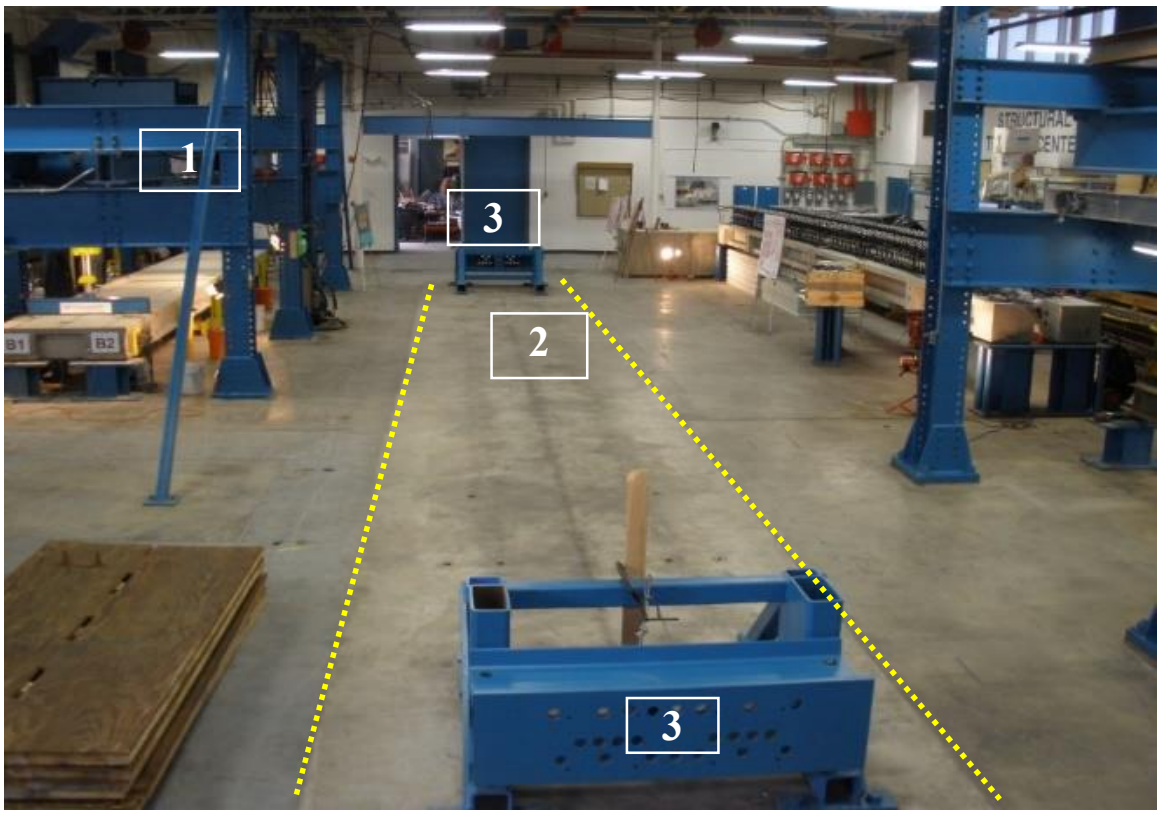

Figure 2.4-2 Structural Testing Center (STC) overview

2.4.2 Construction of formwork

As shown in Figure 2.4-3, each decked bulb T beam had a total length of 41 ft and was provided with seven equally spaced diaphragms at a spacing of 6.5 ft. The decked bulb T beams were cast side-by-side within the two prestressing beds in the STC and CIMR. Figure 2.4-4 shows the general layout for two beams during construction. The formwork for the beams included a wood platform decking system and the sides of the formwork. The decking platform was constructed of plywood and dimension lumber. Figure 2.4-5 shows the decking system. A laser level was used to level the entire platform, which had a total length of 42 ft and a total width of 4 ft to accommodate two decked bulb T beams. The sides of the formwork were constructed from layers of plywood and polystyrene (Styrofoam) to form the required bulb T shape and accommodate the diaphragms. This construction approach allowed for flexibility in creating any shape desired within the constraints of the wood support system. Deforming was another concern for choosing the polystyrene, due to the ease of removing after casting concrete. The extruded polystyrene was replaced with every beam constructed, while the wood support structure was reused throughout the entire experimental phase. Figure 2.4-6 shows the polystyrene layers adhered together and attached to the plywood. These layers of polystyrene were pre-cut to shape using a table saw and attached to the plywood using adhesive and wood screws.

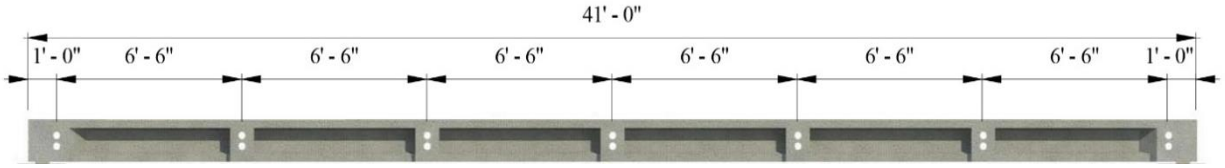

Figure 2.4-3 Longitudinal view of a decked bulb T beam

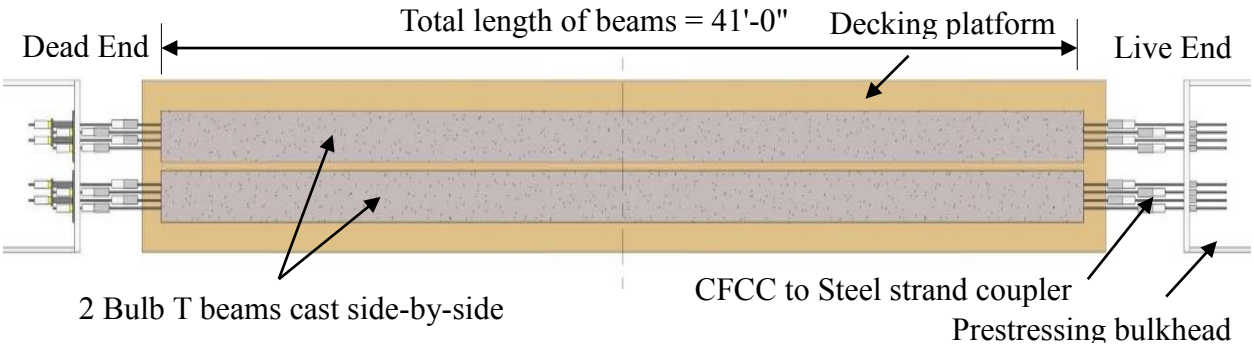

Figure 2.4-4 General layout of decked bulb T beam during construction

Figure 2.4-5 Wood platform decking system

Figure 2.4-6 Construction of formwork using layers of polystyrene and plywood

2.4.3 Reinforcement cages

The reinforcement cages were made of the stirrups and the non-prestressed strands/reinforcement. As mentioned earlier, all control beams other than C-C-S-B included steel stirrups, while Beam C-C-S-B included CFCC stirrups. The steel stirrups were made of two pieces welded together with tack welds as shown in Figure 2.4-7. Similarly, CFCC stirrups were made of two pieces tied together with heavy-duty plastic ties as shown in Figure 2.4-8.

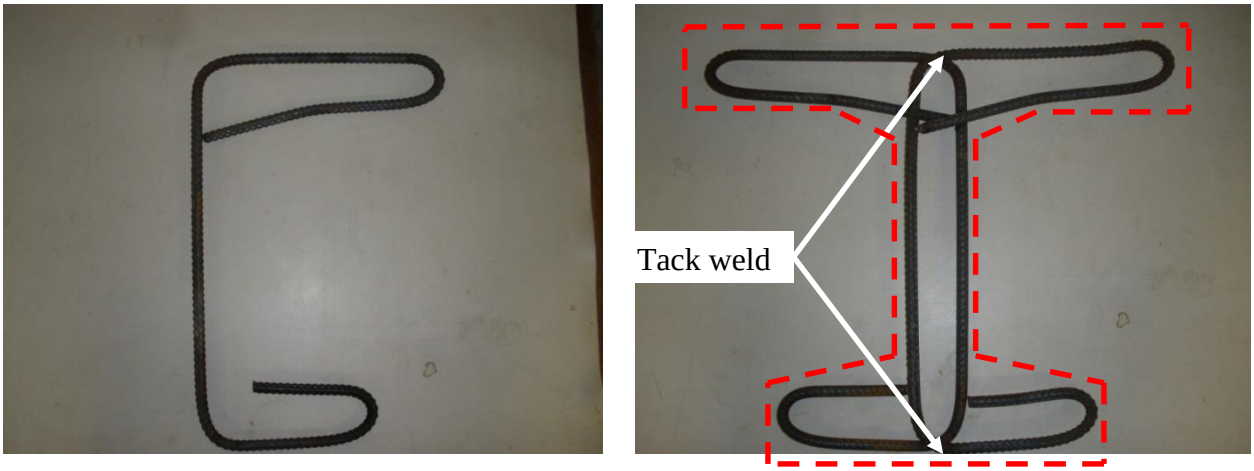

Figure 2.4-7 Steel stirrups of control beams other than Beam C-C-S-B

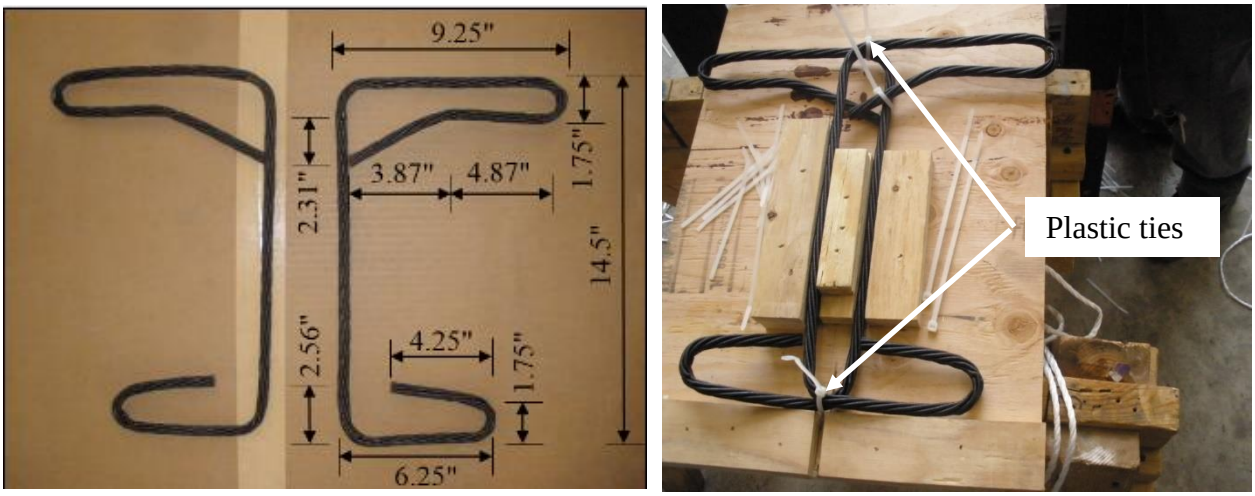

Figure 2.4-8 CFCC stirrups for Beam C-C-S-B

Similar to steel strands, CFCC strands came in rolls as shown in Figure 2.4-9. The research team cut the strands to the required length using air-powered cutting tools or a grinder. The strands were secured to a mount where the stirrups were attached and tied at a spacing of 4 in. as shown in Figure 2.4-10. The transverse diaphragms had additional longitudinal and transverse rectangular stirrups. Similarly, the end blocks were provided with rectangular stirrups every 2.0 in. to resist the bursting force at prestess release. Once reinforcement cages were completed, they were moved to the platform decking, where prestressing strands were passed through the cages as shown in Figure 2.4-11.

Figure 2.4-9 Cutting CFCC strands and constructing reinforcement cages

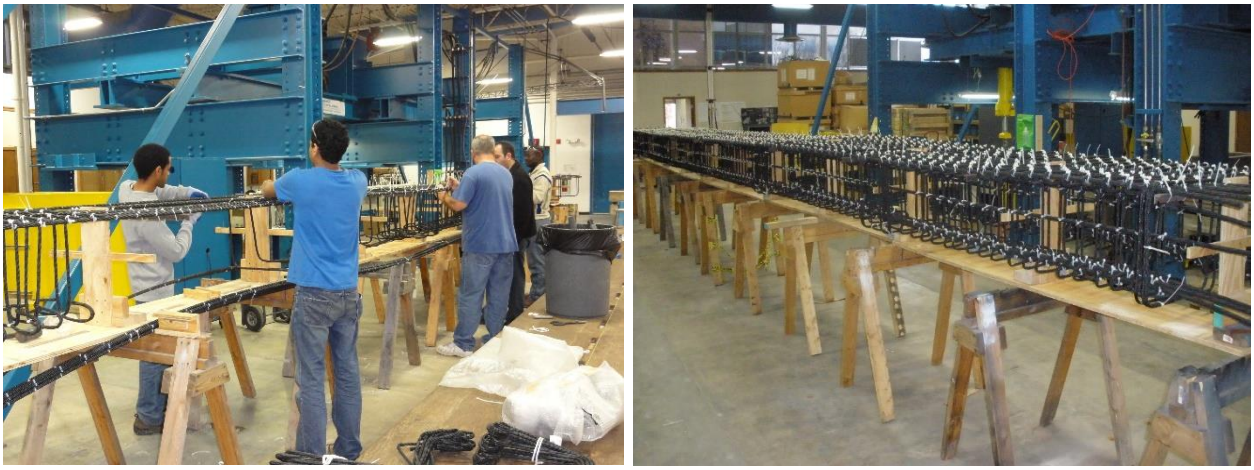

Figure 2.4-10 Building reinforcement cages for control beams

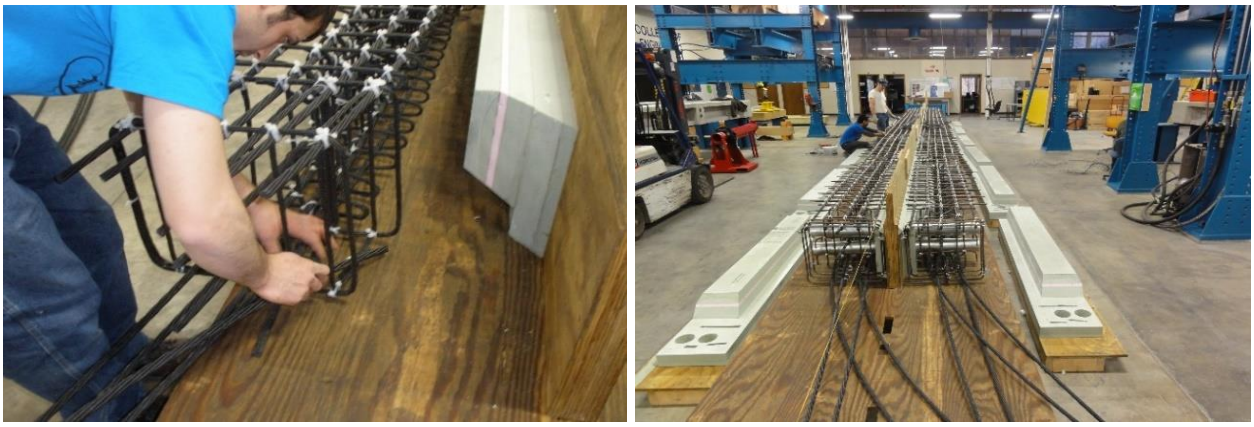

Figure 2.4-11 Moving reinforcement cages to platform decking and passing prestressing strands inside completed cages

2.4.4 Internal instrumentation

All the longitudinal reinforcement including prestressing and non-prestressing reinforcement was instrumented with strain gages at the mid-span for beams tested under flexural loading and under the loading point in Beam C-C-S-B which was tested under shear loading. In addition, each stirrup within the shear span of Beam C-C-S-B was provided with two strain gages. The shear span is defined as the distance from the center line of the support to the loading point. A protective layer was provided around the strain gages to ensure their workability after concrete casting and to prevent moisture penetration to the gage. The used protective layer was either a thick layer of silicon for stirrups or a heat shrink sleeve for longitudinal strands (Figure 2.4-12).

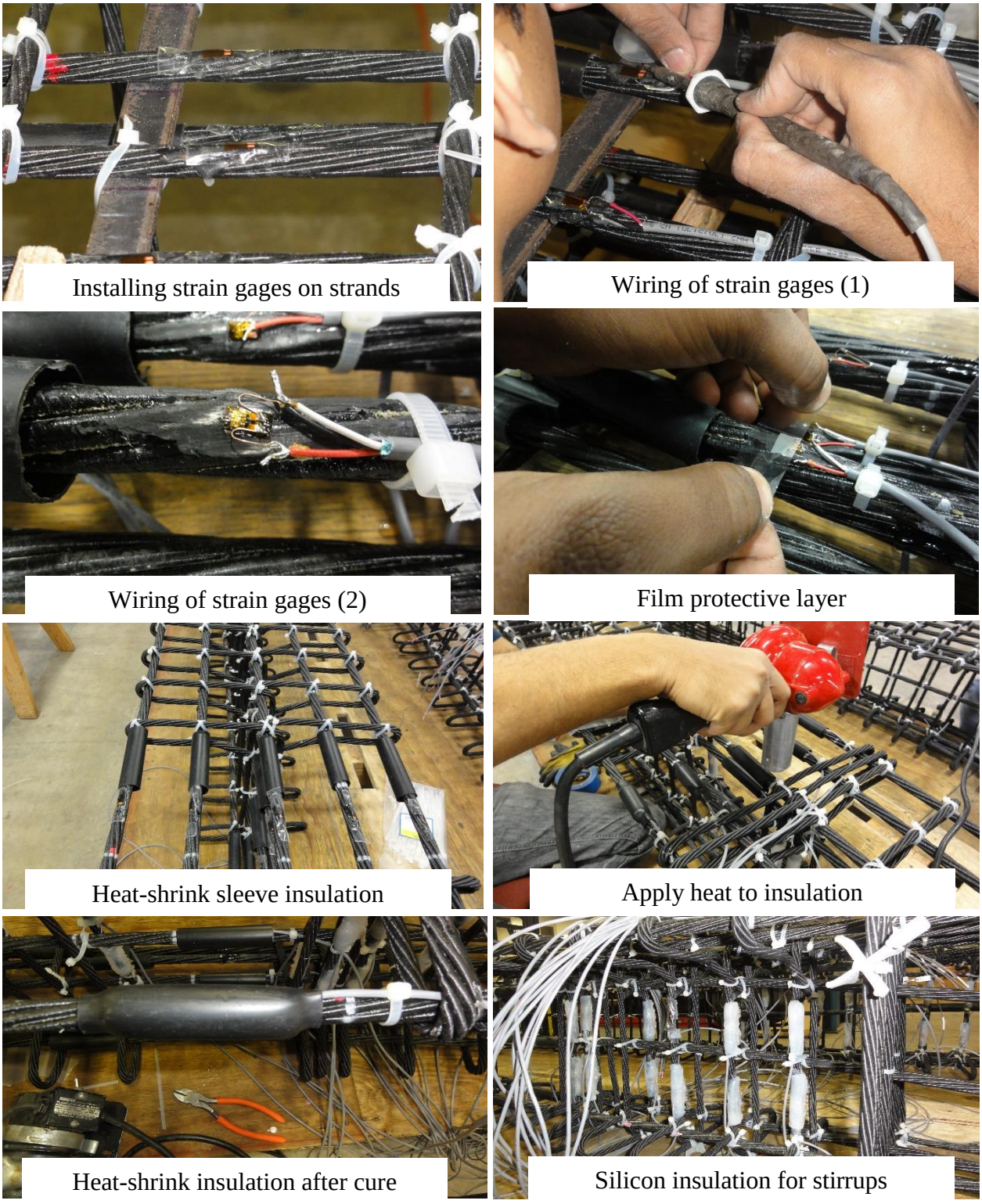

Figure 2.4-12 Internal instrumentation of control decked bulb T beams

2.4.5 Prestressing

To facilitate the process of prestressing and avoid damaging the CFCC strands, a special coupler system (Figure 2.4-13) was developed, tested, and used to connect the prestressing CFCC strands with conventional 7-wire 0.6 in. low relaxation steel strands. The couplers were provided on both the live and dead ends. Therefore, conventional steel anchorage was used at both bulkheads and the prestressing was executed by tensioning the steel strands. The coupler system consisted of two parts (Parts A and B). Part A of the coupler consisted of a high-strength steel barrel encasing a four-steel-wedge system, while Part B consisted of a high strength steel barrel with enough room to accommodate conventional anchorage for steel strands. The CFCC strand was attached to Part A, while the steel strand was attached to Part B. As shown in Figure 2.4-14, to attach the CFCC strand to Part A of the coupler, a buffer material with a steel braided-wire sleeve enclosed the strand to enhance the friction with the four-wedge-steel system. Part A was then fastened to the second barrel (Part B) with a steel strand anchored to it.

Figure 2.4-13 Completed coupler system for prestressing CFCC strands

Attaching buffer material to CFCC strands

Steel braided mesh to increase friction

Four-wedge system inside barrel

Fastening Parts A and B of the coupler

Figure 2.4-14 Coupling CFCC strands with steel strands for prestressing

After completing the installation of the coupler system, the prestressing stage started by tensioning the steel strands at the live end of the prestressing bed. The dead end included load cells to monitor the force. The prestressing was executed by a hydraulic pump and a jacking system, shown in Figure 2.4-15. The strands were prestressed in a predetermined sequence to avoid generating a significant eccentricity of the bulkhead. The initial prestressing force was set to 33 kip/strand. The elongation of each strand was measured and recorded (Figure 2.4-16). The force in each prestressing strand was measured using the reading form the load cell (Figure 2.4-17), the strain gage, the hydraulic pump and the elongation. As shown in Table 2.4-1, at a prestressing level of 33 kip, the elongation of CFCC strands averaged 6 in. while the elongation of steel strands averaged 4 in. A seating loss of 1.5 kip per strand (4.5%) was observed immediately after prestressing. An additional 1.0 kip loss was observed from time of jacking to placement of concrete 24 hours later.

Figure 2.4-15 Prestrssing CFCC strands by tensioning coupled steel strands

Figure 2.4-16 Measuring elongation of strands after prestressing

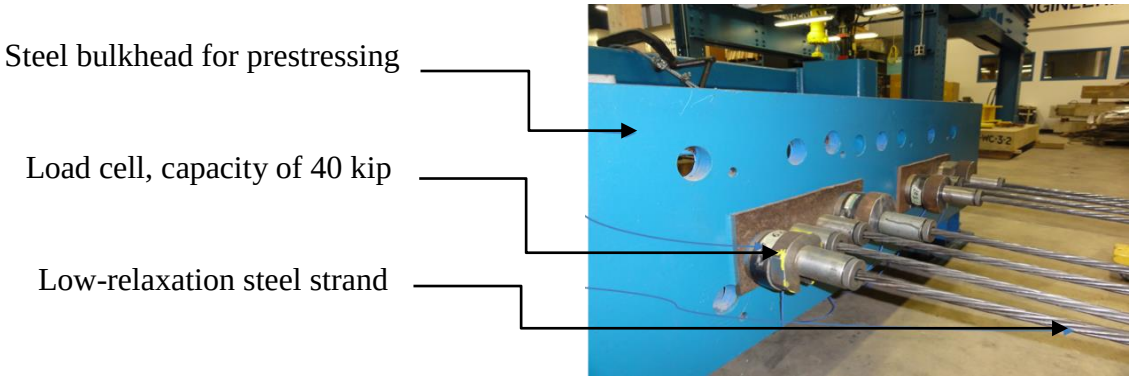

Figure 2.4-17 Load cells on the dead end of prestressing strands

Table 2.4-1 Measured elongation of strands immediately after prestressing

Beam	Elongation (in.)			
	Strand 1	Strand 2	Strand 3	Strand 4
C-S-F-B	6.38	6.38	6.50	6.50
S-S-F-U	4.00	4.00	3.94	4.00
C-C-S-B	6.25	6.25	6.00	6.13
C-S-F-U	6.25	6.13	6.25	5.75
C-S-F-O	6.00	6.00	6.00	5.88
Bridge Beam 1 (exterior)	5.75	5.94	6.38	6.38
Bridge Beam 2 (interior)	6.31	6.38	6.38	5.88
Bridge Beam 3 (intermediate)	5.75	5.75	6.00	6.00
Bridge Beam 4 (interior)	6.25	6.63	6.63	6.50
Bridge Beam 5 (exterior)	6.38	6.13	6.25	5.94

2.4.6 Concrete casting

All the beams were cast using a ready-mix concrete provided by Mc-Coig Concrete Inc. The concrete mix (shown in Table 2.4-2) was designed to achieve a 28-day compressive strength of 7000 psi. The maximum aggregate size was limited to 0.75 in. and a slump of at least 8 in. was imposed on all concrete batches. This concrete mix is a typical concrete mix used in highway bridge beams. Casting of the concrete was performed in CIMR and STC. The concrete was placed in the formwork using a half-cubic-yard hopper's chute and concrete vibrators. Typical casting time for two beams was around 20 minutes. Float troweling, edging, and finish troweling was performed to give a smooth surface finish on top of the beams. Figure 2.4-18 to Figure 2.4-20 show the process of concrete casting.

Figure 2.4-18 Slump test

Table 2.4-2 Concrete mix design

Component	Quantity per cubic yard
Coarse aggregate (L26A-GL)	1710 lb
Fine aggregate (2NS-WLB)	1290 lb
Cement (CMT1-HOL)	534 lb
Cement (CMGS-HOL)	288 lb
Water	31.8 gal
Water reducing agent (0WRA-BA)	24 oz
Medium-range water reducing agent	74 oz

Figure 2.4-19 Casting of concrete into the formwork of two beams

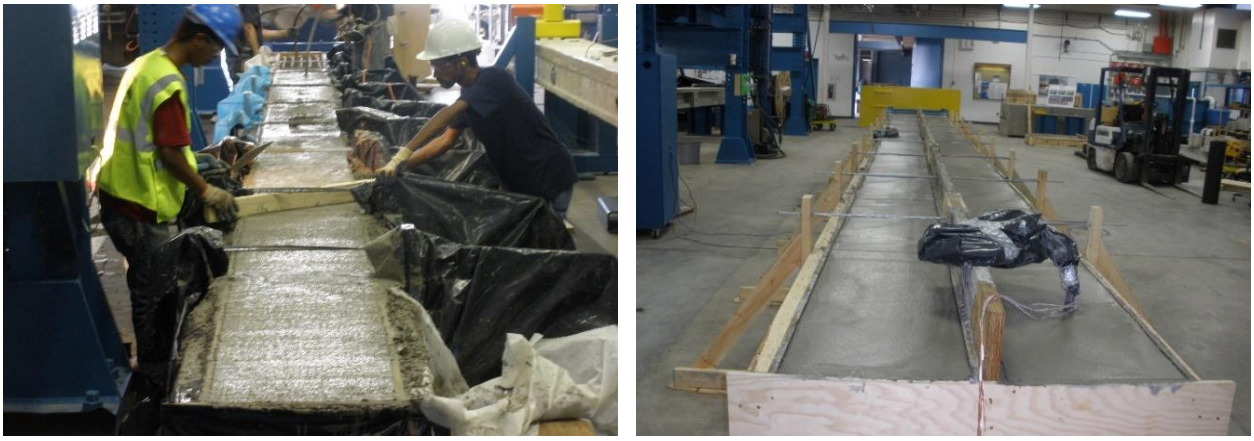

Figure 2.4-20 Leveling and finishing concrete surface

After concrete casting, the beams were covered with wet burlap and plastic sheets to prevent moisture escape and allow for proper curing. The burlap was soaked with water twice a day for seven days (Figure 2.4-21).

Figure 2.4-21 Wet curing of concrete beams

Concrete cylinders with a diameter of 6 in. and a length of 12 in. were also cast from every batch of concrete (Figure 2.4-22). The cylinders were allowed to cure under the same conditions of the concrete beams and were tested under uni-axial compressive stress according to ASTM C39/C39M-12a (2012), Standard Test Method for Compressive Strength of Cylindrical Concrete Specimens, to determine the compressive strength of concrete after 3, 7, 14, 21, and 28 days. In addition, at least three cylinders were reserved and tested on the same day as the corresponding beam testing. Table 2.4-3 gives the average compressive strengths, obtained from testing at least three cylinders, for the batches of concrete used during this investigation.

Table 2.4-3 Average concrete compressive strength at different ages

Beam	Compressive Strength (psi)			
	7 Day	14 Day	21 Day	28 Day
C-S-F-B	6580	7302	7598	7684
S-S-F-U	5728	6248	8404	8746
C-C-S-B	7356	7685	8623	8648
C-S-F-U & C-S-F-O	6866	7566	8869	9438
Bridge Beams 1, 2, 3, 4	7085	7448	8569	8995
Bridge Beam 5	6563	7617	8296	8780

Figure 2.4-22 Concrete cylinders and uni-axial compression test

2.4.7 Prestress release

Transfer of prestressing forces into concrete beams took place 10 days after casting of concrete and after verifying that the concrete had achieved more than 60 % of its 28-day compressive strength. The prestress release was executed by slowly heating the steel strands using an acetylene/oxygen torch as shown in Figure 2.4-23. The exterior strands of each beam were released before the interior strands. A heavy duty wooden cover was placed over the CFCC anchors to eliminate any hazards to the anchors and the person holding the torch. The camber of the beams was measured at the mid-span of the beam at prestress release. Figure 2.4-24 shows the camber of the beams measuring approximately 0.75 in. After prestress release, the beams were removed from the formwork and sent to either the testing facility or to indoor storage until a testing facility was available. While moving, the beams were simply supported as shown in Figure 2.4-25.

Figure 2.4-23 Prestress release using acetylene/oxygen torch

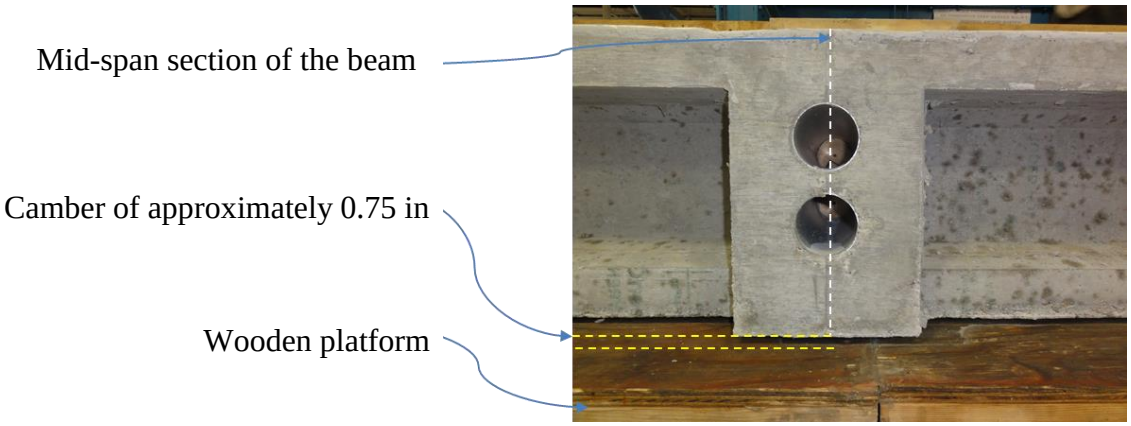

Figure 2.4-24 Camber of beam at mid-span immediately after prestress release

Figure 2.4-25 Moving the beams from the formwork to the loading facility

2.5 Construction details of bridge model

The main two phases of the bridge model construction were:

1. Construction of the individual decked bulb T beams
2. Assembling the bridge model from the individual beams using shear key connections.

As shown in Figure 2.5-1, Figure 2.5-2, and Figure 2.5-3, the bridge model consisted of five decked bulb T beam with two end diaphragms and five intermediate diaphragms. Part of the diaphragms was cast along with the beams and then the diaphragms were connected together using UHPC. Each intermediate diaphragm was reinforced with 4 No.3 reinforcing bars. These bars were spliced before pouring the UHPC. The end diaphragms and the intermediate diaphragms were also provided with galvanized steel conduits with a diameter of 3 in. to accommodate the transverse

post-tensioning strands. The following subsections provide a summary for the stages of construction of the bridge model.

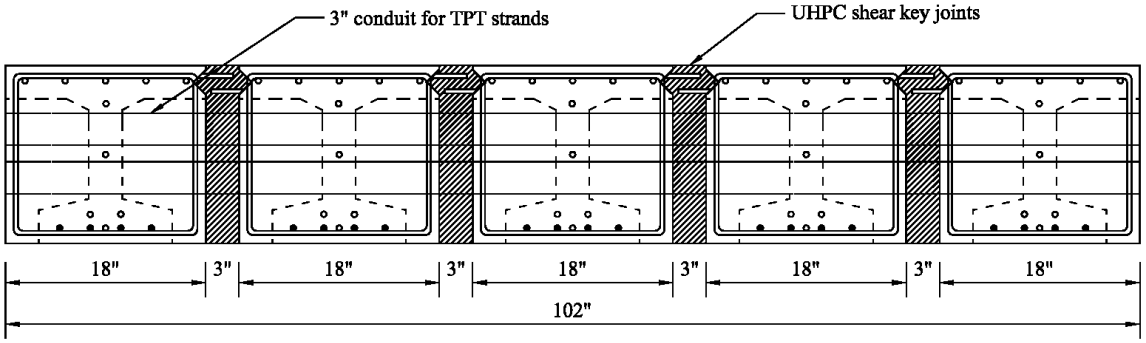

Figure 2.5-1 Cross section of bridge model at end diaphragms

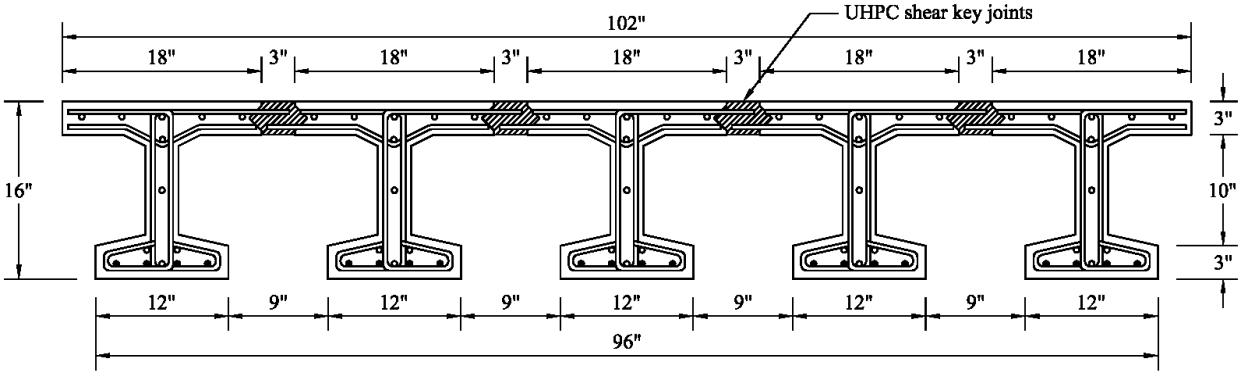

Figure 2.5-2 Cross section of bridge model between diaphragms

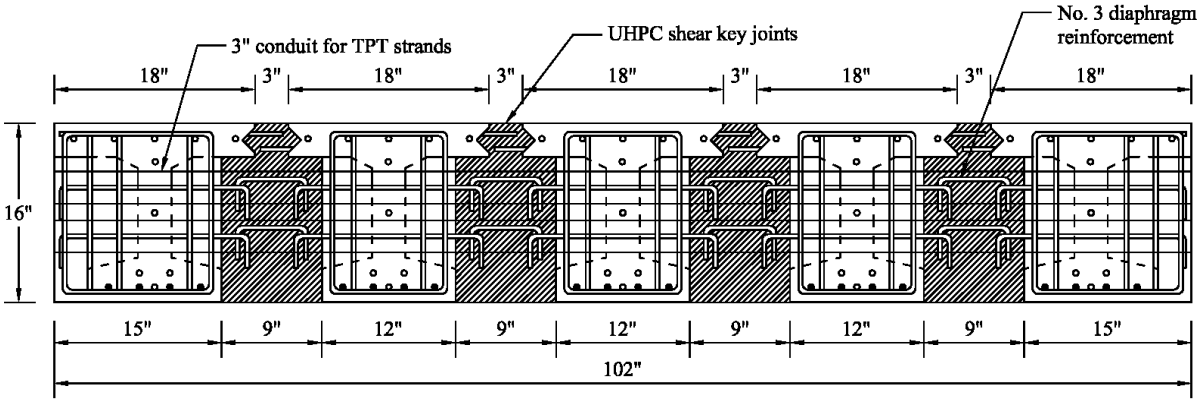

Figure 2.5-3 Cross section of bridge model at intermediate diaphragms

2.5.1 Construction of individual beams

The beams of the bridge model were identical in reinforcement to Beam C-S-F-B, with four bottom prestressed CFCC strands and three bottom non-prestressed CFCC strands in addition to five top non-prestressed CFCC strands and two web CFCC strands. In the transverse direction, the beams were also reinforced with steel stirrups at a center-to-center spacing of 4 in. However, the stirrups protruded the top flange of the beams and extended to a distance of 2.5 in. to form the required reinforcement of the shear key joints. The exterior beams had the protrusion from the interior side only while the interior beams had the protrusion from both sides as shown in Figure 2.5-4 and Figure 2.5-5.

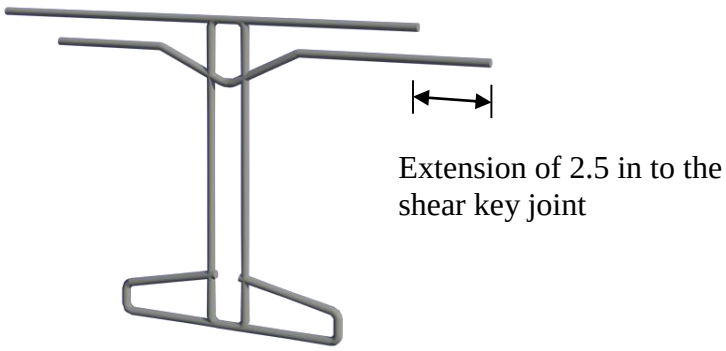

Figure 2.5-4 Steel stirrup for interior beams in bridge model

Figure 2.5-5 Sides of the formwork showing protrusion of steel stirrups for form shear key reinforcement in bridge beams

This protrusion of stirrups was accommodated during the construction of the sides of the formwork by drilling holes in the polyethylene and plywood layers as shown in Figure 2.5-5. In addition, the transverse reinforcement of the diaphragms also protruded of the concrete, mainly to facilitate the splice of reinforcement while assembling the bridge model. This protrusion was also accommodated during the construction of the formwork. Apart from this modification in the formwork, the construction of the individual beams of the bridge model went through the same construction stages of the control beams. Therefore, it will not be repeated in this section. The elongation of the prestressing strands at the time of prestressing is provided in Table 2.4-1, while the compressive strength of concrete at different ages was provided in Table 2.4-3.

2.5.2 Construction of shear key joints

2.5.2.1 Material testing

Prior to the construction of the shear key joints in the bridge model, small-scale specimens of UHPC joints were prepared and tested to failure. Eight specimens were prepared and tested according to ASTM C78-10 (Flexural strength of concrete using simple beam with third-point loading); ten specimens were prepared and tested according to ASTM C882-05 (Bond strength of epoxy-resin systems used with concrete by slant shear); and four specimens were prepared and tested according to ASTM C1583-04 (Tensile strength of concrete surfaces and the bond strength by direct tension, pull-off method). The standard tests were slightly modified to fit the intended application of UHPC in shear key joints. Figure 2.5-6 to Figure 2.5-8 show the configuration of the test specimens. The ASTM C78 specimens were prepared by connecting two 8 in. × 6 in. × 12 in. concrete blocks using a 3.0 in. wide flat or notched UHPC shear keys. The ASTM C882 specimens were prepared by casting 3 in. × 6 in. cylinders of concrete/UHPC. The ASTM C1583 specimens were prepared by connecting two 4 in. × 8 in. cylinders with an UHPC joint.

All test specimens were prepared by: first, pouring the concrete components; second, allowing enough time for curing; third, sand blasting and water saturating the surfaces; and finally, mixing and pouring the UHPC joints between concrete components. After pouring the UHPC joints, the test specimens were allowed to cure for 28 days before testing. On the day of the test, the concrete achieved an average compressive strength of 6 ksi, while the UHPC achieved a compressive strength of 21 ksi.

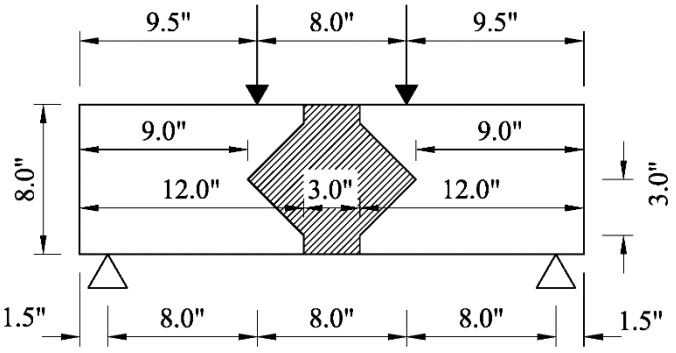

Figure 2.5-6 Details of test specimens for ASTM C78 with notched joint

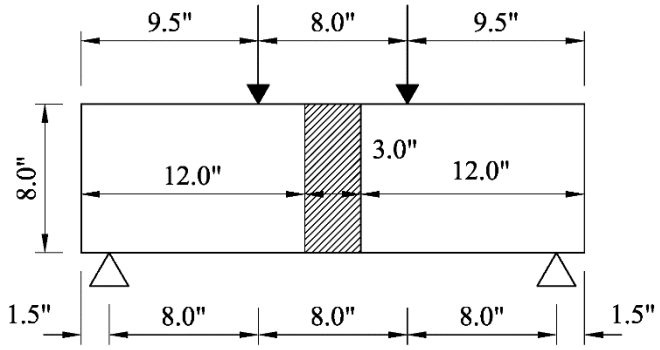

Figure 2.5-7 Details of test specimens for ASTM C78 with flat joint

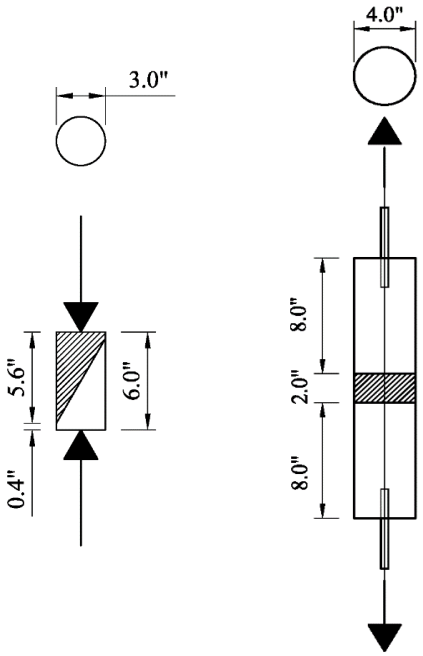

Figure 2.5-8 Details of test specimens for ASTM C882 (left), and ASTM C1583 (right)

Specimens tested under ASTM C78 with flat shear keys achieved an average failure load of 12.3 kip with an average flexural stress of 768 psi at the bottom surface of the specimens. Specimens tested under ASTM C78 with notched shear key achieved an average failure load of 16.4 kip with an average flexural stress of 1,027 psi. It should be noted that the apparent increase in the failure load in specimens with notched shear key was associated with the shift of the failure plane from the central region of the specimen toward the end of the specimens as shown in Figure 2.5-9.

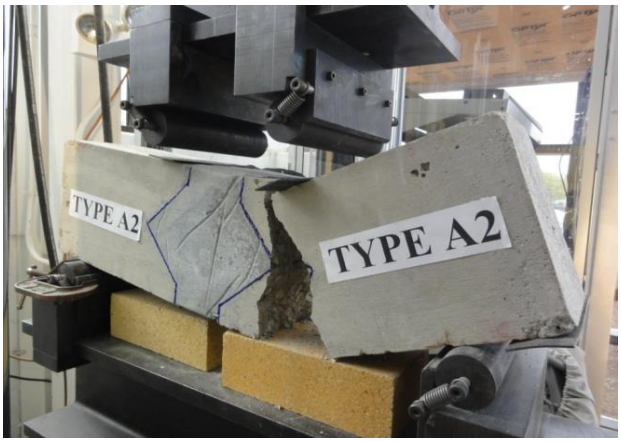

ASTM C78 with notched joint

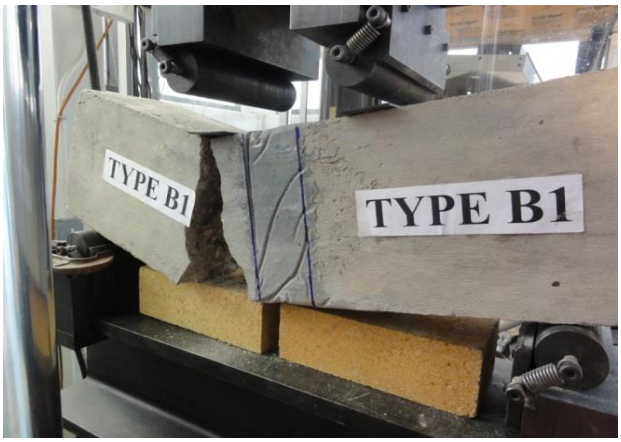

ASTM C78 with flat joint

ASTM C882

ASTM C1583

Figure 2.5-9 Failure and failure planes of UHPC joints under ASTM tests

Specimens tested under ASTM C882 achieved an average failure load of 71.5 kip with average bond strength at the concrete/UHPC interface of 5.1 ksi, considering an elliptical interface with an area of 14.13 in.^{2} according to ASTM C882. On the other hand, specimens tested under C1583

achieved an average failure load of 5.4 kip with an average direct tensile stress of 426 psi. As shown in Figure 2.5-9, the failure plane in all test specimens was always on the concrete side. Therefore, the provided stress values represented the maximum strength of the concrete and not the UHPC or the interface between the concrete and the UHPC. Consequently, it was concluded that the bond strength at the concrete/UHPC interface exceeded the strength of the concrete material. Accordingly, the research team gained confidence in the strength of the UHPC joints and proceeded with using the UHPC to form the shear key joints in the bridge model.

2.5.2.2 Surface preparation

The surface preparation for the decked bulb T beams included sandblasting the surface of the shear key joints and the face of the transverse diaphragms. The sandblasting was performed by spraying fine sand using air-powered spray nozzle as shown in Figure 2.5-10.

Figure 2.5-10 Sandblasting surfaces of the shear key joints

2.5.2.3 Placing UHPC Shear keys

After completing the sandblasting, the beams were set in position over the supports with a 3.0-in. gap between the beams as shown in Figure 2.5-11. Next, the differential camber of the beams was evened out using two steel beams connected together with steel threaded rods as shown in Figure 2.5-12. This process was necessary to create a smooth riding surface for the bridge. It should be noted that the differential camber between beams measured less than 0.1875 in. These steel beams were removed after casting and curing of UHPC shear-key joints.

After leveling the beams, the research team constructed the formwork for the shear key joints. The formwork extended beneath the shear keys and around the transverse diaphragms (Figure 2.5-13). In addition, to prevent the UHPC from seeping into the ducts of the transverse post-tensioning, galvanized steel pipes with a diameter of 2.5 in. was inserted inside the 3.0-in. pipes that passed through the body of the beams (Figure 2.5-14).

Figure 2.5-11 Setting beams over the supports with 3.0-in. gap for shear keys

Figure 2.5-12 Beam leveling to eliminate differential camber

Figure 2.5-13 Formwork for shear key joints and around transverse diaphragms

Figure 2.5-14 Continuous steel pipe to prevent UHPC leakage into transverse ducts

The UHPC was prepared at CIMR by mixing together: 3700 lb of Ductal premix, 219.1 lb of water, 50.6 lb of superplasticizer (Premia 150), and 262.9 lb of brass-coated steel fibers as shown in Figure 2.5-15. A centrifugal concrete mixer was used to mix the components for at least 25 minutes until the mix became homogeneous (Figure 2.5-16). The mixing of Ductal was executed by feeding the pre-mix powder to the mixer and then adding the water and the water reducing agent. The steel fiber was the last component added to the mix.

Each batch of UHPC provided by Lafarge was tested to ensure quality control throughout the casting. Figure 2.5-17 shows the setup for cylinder casting and flow table testing of batches. A count of 25 blows was performed according to ASTM C1437, Standard Test Method for Flow of Hydraulic Cement Mortar. The diameter of the sample after the 25 blows was approximately 9.0 in., which fell within the acceptable range of workability for the material.

Pouring the UHPC to the shear key joints was performed manually as shown in Figure 2.5-18. As the UHPC is characterized with its flowing and self-leveling ability, there was no need to use a vibrator or float the surface.

After pouring, the shear key joints were covered with plastic sheets and allowed to cure at ambient temperature for 72 hours (Figure 2.5-19). After curing, the surface of the joints was grinded using a drum grinder to achieve an even bridge surface as shown in Figure 2.5-20.

Pre-mix powder for UHPC

Water reducing agent

Coated steel fibers

Concrete mixer

Figure 2.5-15 Items used to prepare UHPC

Figure 2.5-16 Mixing UHPC

Figure 2.5-17 Flow test for UHPC according to ASTM C1437

Figure 2.5-18 Pouring UHPC shear key joints

Figure 2.5-19 Curing of shear key joints using plastic sheets

Figure 2.5-20 Grinding the surface of UHPC shear key joints

2.5.3 Transverse post-tensioning

The bridge model was provided with seven transverse diaphragms. Each diaphragm hosted two transverse ducts to accommodate two CFCC transverse post-tensioning strands. The anchorage devices (threaded sleeve and lock nut) for the strands were already attached by the manufacturer (Figure 2.5-21). However, to distribute the post-tensioning force over the diaphragm area and eliminate the concentration of the stress, steel bearing plates with a thickness of 2 in. were attached to the exterior sides of the diaphragms. The post-tensioning strands were passed through the transverse ducts and had their lock nuts bearing against the steel plates. The post-tensioning force was applied using a hydraulic pump and a jacking system. To monitor the post-tensioning force, load cells were sandwiched between two steel plates as shown in Figure 2.5-22.

Figure 2.5-21 Transverse post-tensioning system with pre-attached sleeve-and-nut anchorage

Figure 2.5-22 Load cells to monitor the transverse post-tensioning force

2.6 Sensors and data acquisition system

The sensors used in the study included internal strain gages on CFCC strands, external strain gages on concrete, linear motion transducers (LMT) for deflection measurements, and load cells. All sensors were connected to a data acquisition system as shown in Figure 2.6-1 and Figure 2.6-2 . As shown in the figure, the sensors were connected to the central processing units, which transform the analog electrical pulses from the sensors to digital signals recorded and stored in a laptop computer equipped with the data acquisition software "Mars Labs".

The strain gages on the concrete had a length of 2.0 in. The length was selected to be larger than twice the maximum aggregate size of the concrete mix (0.75 in.). The gages were attached to the surface of the concrete using special epoxy adhesive after preparing the surface. Through the flexural testing of the control beams and the bridge model, the strain gages were attached to the top surface of the concrete at the mid-span and next to the two loading points of the four-point loading setup. The load was applied through a 220 kip MTS hydraulic actuator with a maximum stroke of 20 in. The actuator was programmed to deliver load by displacement control at a rate of 0.25 in/min. In addition, load distribution tests on the bridge model was performed using a 100-ton hydraulic cylinder with a stroke of 10 in. The LMTs performed as expected and were able to capture the deflection of the test specimens. In addition, Mitutoyo 3.0-in. dial gages with an accuracy of ± .005 in. (Figure 2.6-3) were also used in testing the bridge model under service loads. The dial gages accurately captured the small deflection of the bridge model under service loads without experiencing the electrical noise associated with using electrical sensors.

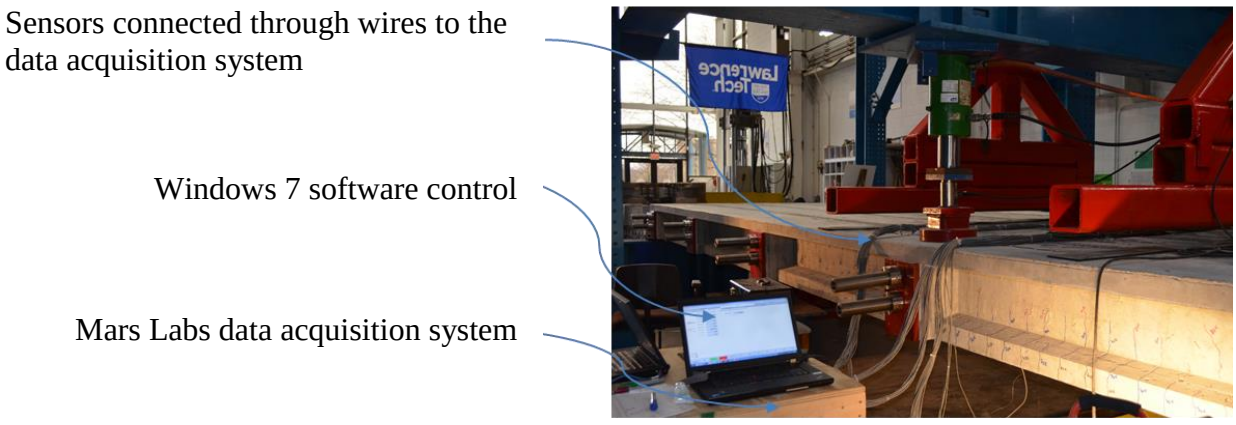

Figure 2.6-1 Data acquisition system wired into bridge model sensors

Figure 2.6-2 Mars Labs Titan model field pods for data acquisition

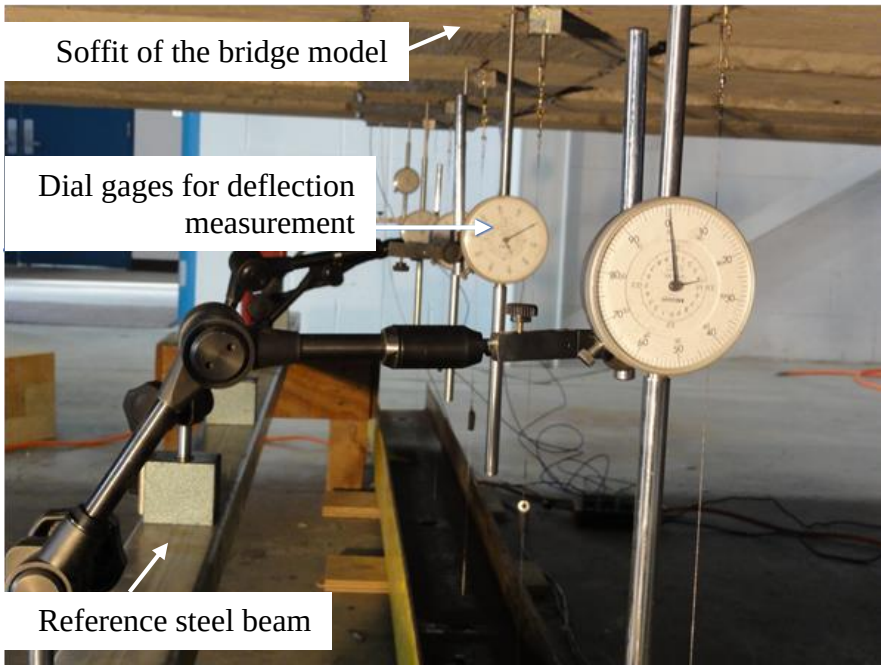

Figure 2.6-3 Dial gages to measure deflection under service loads